Quaternary Science Reviews 230 (2020) 106142

Contents lists available at ScienceDirect

Quaternary Science Reviews

journal homepage: www.elsevier.com/locate/quascirev

Carbon, nitrogen, and oxygen isotopes of ostrich eggshells provide site-scale Pleistocene-Holocene paleoenvironmental records for eastern African archaeological sites

E.M. Niespolo [a, b, *], W.D. Sharp [b], C.A. Tryon [c], J.T. Faith [d, e], J. Lewis [f, g], K. Ranhorn [j], S. Mambelli [h], M.J. Miller [i], T.E. Dawson [h]

[a] Department of Earth and Planetary Science, University of California, Berkeley, CA, USA
[b] Berkeley Geochronology Center, Berkeley, CA, USA
[c] Department of Anthropology, University of Connecticut, Storrs, CT, USA
[d] Natural History Museum of Utah, University of Utah, Salt Lake City, UT, USA
[e] Department of Anthropology, University of Utah, Salt Lake City, UT, USA
[f] Turkana Basin Institute, Stony Brook University, Stony Brook, NY, USA
[g] Department of Anthropology, Stony Brook University, Stony Brook, NY, USA
[h] Department of Integrative Biology, University of California, Berkeley, CA, USA
[i] Archaeological Research Facility, University of California, Berkeley, CA, USA
[j] School of Human Evolution and Social Change, Arizona State University, Tempe, AZ, USA

ARTICLE INFO

Article history:
Received 4 July 2019
Received in revised form
16 December 2019
Accepted 20 December 2019
Available online xxx

Keywords:
Africa
Stable isotopes
Ostrich eggshell
Quaternary paleoecology
Paleoclimatology
Middle Stone Age
Later Stone Age

ABSTRACT

Quantitative, well-dated, local paleoenvironmental records are necessary to 1) evaluate responses to regional to global-scale climate change at the scale of human habitats, and 2) test hypotheses regarding the effects of environmental change and human biological and cultural evolution. Ostrich eggshell (OES) fragments are common in African archaeological sequences, are amenable to ^{14}C and $^{230}Th/U$ dating, and their stable carbon ($\delta^{13}C$ values) and nitrogen ($\delta^{15}N$ values) isotopic compositions track local vegetation and mean annual precipitation (MAP), respectively. We review previous interpretations of the stable isotopic composition of OES, apply a novel calibration to estimate paleo-MAP (PMAP) from $\delta^{15}N$ values, and show that oxygen isotopes ($\delta^{18}O$ values) record evapotranspiration, which is controlled by temperature, relative humidity, and/or photosynthetic performance, if other components of the water cycle are constrained. The stable isotopic compositions of the organic fraction of OES remain unaltered to at least ~50 ka, indicating potential to examine even older OES. We present a ~50–4 ka record of OES $\delta^{13}C$, $\delta^{15}N$, and $\delta^{18}O$ values from archaeological sites recording the Middle to Later Stone Age (MSA/LSA) transition at Lukenya Hill (Kenya) and Kisese II (Tanzania). Stable isotope proxies indicate contrasting but subtle changes in local paleoenvironment throughout the records at both sites, likely explained by local ecological and climatological effects that are not resolved by regional-scale paleoclimate records. These records highlight the need for additional local studies to assess the covariance of paleoenvironments and material culture. Furthermore, they indicate that the MSA/LSA transition at the two sites did not result from paleoenvironmental change.

1. Introduction

Archaeological and climate records are often spatially and temporally discontinuous, particularly in eastern Africa (Blome et al., 2012). Proxy records from ice, marine, and lake cores are commonly used to assess relationships between climatic and human behavioral change (e.g., Jones and Stewart, 2016; Tierney et al., 2017; Timmermann and Friedrich, 2016; Ziegler et al., 2013), even though they represent large scale (>10^2 km^2) changes. Eastern African lacustrine records are more proximal but still may be remote from archaeological deposits; thus, they are difficult to correlate with archaeological sequences due to varying

* Corresponding author. Department of Earth and Planetary Science, 307 McCone Hall, MC4767, Berkeley, CA, 94720, USA.
E-mail addresses: eniespolo@berkeley.edu, niespolo@caltech.edu (E.M. Niespolo).

https://doi.org/10.1016/j.quascirev.2019.106142
0277-3791/

chronological resolution between records and they may not resolve environmental change at scales directly relevant to archaeological sites (i.e., $<10^2$ km^2; e.g., Kelly, 2013). The region of eastern Africa today is characterized by rainfall regimes that differ spatially in both amount and seasonality, and combined with highly variable bedrock geology and topography, these factors have created a heterogenous patchwork of local environments that can vary across scales of 10^1–10^3 km (e.g., Adams et al., 1996; Lind and Morrison, 1974; Shorrocks, 2007; White, 1983). The extent to which the present pattern of intra-regional environmental variability can be extended into the past is unknown, but comparison of long-term data from eastern African lacustrine records has suggested contrasting trends towards either increased aridity (Owen et al., 2018) or increased humidity (Johnson et al., 2016) throughout the Late Pleistocene.

In contrast, paleoenvironmental records retrieved from dated archaeological sequences can facilitate hypothesis testing regarding climate and changes in human behavior. For example, the shift from Middle Stone Age (MSA) to Later Stone Age (LSA) technologies represents a fundamental change in the Late Pleistocene African archaeological record and is widely thought to play an important role in understanding the origin and dispersal of modern humans (*Homo sapiens*). This is because (1) genetic and fossil data support an African origin for our species, possibly in eastern Africa, with a key interval of several out-of-Africa dispersals occurring 40–60 thousand years ago (ka) (Henn et al., 2018; Mallick et al., 2016), (2) the earliest LSA assemblages in eastern Africa date to 40–60 ka (Ambrose, 1998; Gliganic et al., 2012; Tryon et al., 2018), and (3) early Eurasian Upper Paleolithic assemblages associated with fossil *H. sapiens* share broad technological similarities to early LSA ones, particularly in the production of smaller, blade and bladelet-based assemblages, and greater use of ochre colorants and items of personal adornment (Klein, 2008). Why the MSA/LSA transition occurred remains poorly understood, although the timing of transition varies across Africa, from as early as ~60–70 ka (Brown et al., 2012; Gliganic et al., 2012), to perhaps as late as the Holocene (Bahain et al., 2017). This may be due to multiple interrelated phenomena, including (1) local innovations in response to changes in the immediate environment, (2) the presence of larger and more dense human populations, (3) the spread of new ideas through existing social networks, or (4) population dispersals across Africa prior to and coincident with out-of-Africa expansions (Tryon, 2019; Tryon and Faith, 2016).

Furthermore, while evidence from MSA archaeological sites reveals the diverse array of ecosystems available to humans at Middle and Later Stone Age sites, these sites are spatially unevenly distributed across different biogeographic zones (Tryon and Faith, 2013), and detailed study of them has indicated that there may be variable habitat-scale responses to larger scale climate change (Ambrose, 2001; Blome et al., 2012). While the analysis of archaeologically recovered faunal assemblages and local sedimentology are among the most robust records of *qualitative* local environmental change (e.g., wet v. dry), there are few ways to assess *quantitative* changes (e.g., precipitation amounts) without local isotopic data (e.g., Cerling et al., 2011; Cerling and Hay, 1986; Levin et al., 2006; Robinson, 2017).

Given such regional- and continental scale environmental variability throughout the Late Pleistocene (Blome et al., 2012), our study of possible environmental drivers for archaeological change begins at the archaeological site. When stratigraphically associated with other archaeological materials, ancient ostrich eggshell can characterize past local environments at geographic and temporal scales relevant to human subsistence. The carbon (C) and nitrogen (N) stable isotope compositions of well-preserved ostrich eggshell provide quantitative proxies for consumed vegetation and mean annual precipitation (MAP), respectively (Johnson et al., 1998; Von Schirnding et al., 1982). Below, we discuss ostrich (O) eggshell oxygen isotopes, how they may relate to local environmental variables, and present a model to estimate evapotranspiration (related to temperature, relative humidity, and plant photosynthetic pathway). We evaluate the primary preservation and proxy relationships of each isotopic record (δ^{13}C, δ^{15}N, and δ^{18}O values) in ostrich eggshell and show that archaeologically recovered ostrich eggshell fragments can retain primary compositions to at least ~50 ka in eastern Africa. By applying interpretations of established (C, N) and novel (O) stable isotope compositions of ostrich eggshells (OES), we characterize local paleoenvironments of archaeological rockshelter localities in eastern Africa, at Lukenya Hill sites GvJm 22 and GvJm 16 (Kenya) and Kisese II (Tanzania), recording ~50 ka of human occupation. The last 50 ka include various climatic and archaeological changes such as the Last Glacial Maximum, the African Humid Period, and the MSA/LSA transition at these sites. We assess the presence of isotopic signatures of major climate events recorded in the local paleoenvironmental records from Lukenya Hill and Kisese II, compare them to lacustrine records >100 km away, and discuss possible dynamic mechanisms responsible for inferred paleoenvironmental changes. The isotopic proxies for past vegetation, precipitation, and evapotranspiration also allow us to directly examine if local environmental characteristics were similar or distinct at the two sites during the MSA/LSA transition and whether environments were characterized by extreme or rapid changes during or leading up to the MSA/LSA transition.

2. Background

2.1. Stable isotopes of ostrich eggshells as paleoenvironmental proxies

Ostrich (*Struthio camelus)* eggshell fragments accumulate at archaeological sites through human use, transport, and discard. Ostrich eggs can serve as a food source, and ethnographic and Late Pleistocene-Holocene examples demonstrate additional uses of the shells as canteens (sometimes decorated with incisions) and as raw material for the production of beads (e.g., Henshilwood et al., 2014; Texier et al., 2013; Wilmsen, 2015). Because ostriches are broadly unselective feeders, the isotopic compositions of their eggshells reflect local environmental parameters where they obtain their food (Milton et al., 1994). The carbon, nitrogen, and oxygen isotopic compositions of ostrich eggshells are determined by the *local* environment because the home range of daily food sources of ostriches is ~85 km^2 (Milton et al., 1994; Williams et al., 1993). This distance is within both the geographic range of transport of MSA obsidian tools (e.g., Blegen, 2017; Tryon and Faith, 2013) and the home ranges expected for equatorial foragers (Kelly, 2013).

Eggshells rapidly form in <24 h (Nys et al., 2004, 1999) and their stable isotope composition reflects a snapshot of the ostrich diet of the prior ~3–5 days (Johnson et al., 1998). Ostriches lay eggs annually over a period of ~2 weeks after the rainy season (Leuthold, 1976; Moreau, 1950; Sinclair, 1978). Even in regions with bimodal rainfall, all but one modern subspecies of ostrich (*S. camelus molybdophanes*) lay eggs in only one breeding season per year, typically a few months after the long rainy season in eastern Africa (March–May; Leuthold, 1976). Northern Tanzania as well as the highland regions of central Kenya, where our study sites are located, receive rainfall in two phases, as short events October–December and longer, more intense events March–May (McSweeney et al., 2012b; McSweeney et al., 2012a). The diverse modern vegetation distribution in this area is shown in Fig. 1 (van

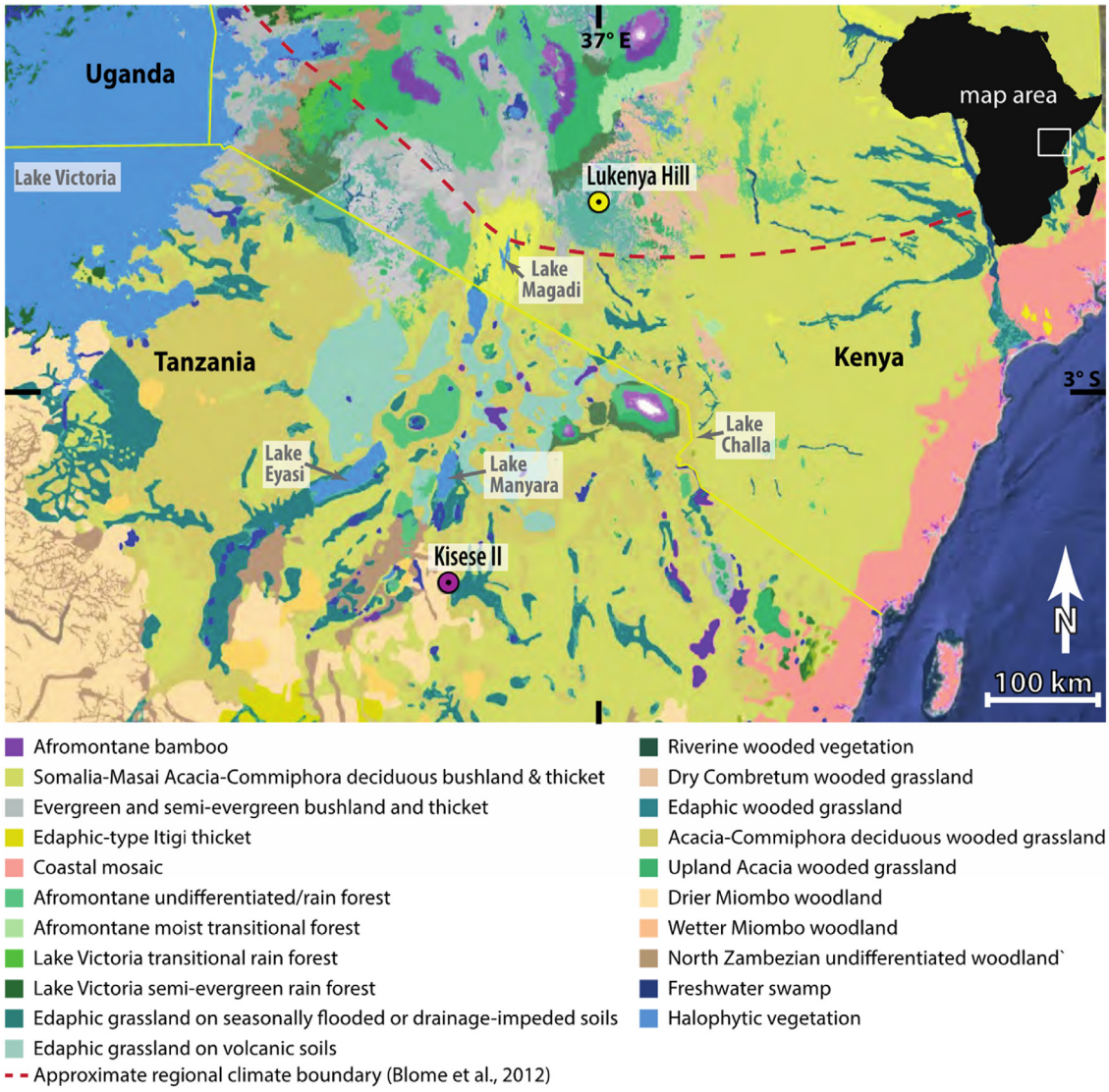

Fig. 1. Map of modern physiognomic vegetation (after van Breugel et al., 2015) showing locations of the Lukenya Hill and Kisese II rockshelters and nearby lakes. Lukenya Hill is surrounded by an extensive edaphic grassland but is within <50 km of other diverse vegetation, while Kisese II is immediately surrounded by diverse vegetation. Vegetation map after van Breugel et al., 2015; map constructed using Google Earth.

Breugel et al., 2015). Below we outline previous efforts to understand each isotope paleoenvironmental proxy. A list of commonly used terms, with reference to these proxy records and those proposed here, is provided in Table 1.

2.1.1. Carbon isotopes in ostrich eggshell

Observations of wild ostriches have shown they are opportunistic water-conserving herbivores that feed almost entirely on green plants within their home range with a slight dietary

Table 1
List of terms and proxy definitions.

Term	Definition	Units
R	ratio of rare to common isotope; e.g.,$^{18}O/^{16}O$	none
δ	$1000 \times \left(\frac{R_{Sample} - R_{Standard}}{R_{Standard}}\right) - 1$	‰
$\alpha_{A\text{-}B}$	R_A/R_B	none
$\Delta_{A\text{-}B}$	δ_A-δ_B	‰
$\Delta^{13}C_{calcite\text{-}TOF}$	$\delta^{13}C_{calcite}$ - $\delta^{13}C_{TOF} = 15 \pm 2$	‰
$\delta^{13}C_{diet}$	$\delta^{13}C_{calcite}$ - 16.2	‰
f_{C4}	fraction of C_4 plants consumed	none
PMAP	paleo-mean annual precipitation, using equation (4)	mm/year
$\alpha_{bodyH2O\text{-}calcite}$	1.0379 ± 0.002	none
$\delta^{18}O_{bodyH2O}$	calculated from $\alpha_{bodyH2O\text{-}calcite}$ and $\delta^{18}O_{calcite}$	‰
$\delta^{18}O_{foliarH2O}$ model 1	solve for $\delta^{18}O_{foliarH2O}$ using calculated ostrich $\delta^{18}O_{bodyH2O}$ and equation (5); result derived from $\delta^{18}O_{calcite}$	‰
$\delta^{18}O_{foliarH2O}$ model 2	foliar water $\delta^{18}O$ value calculated from ostrich $\delta^{13}C_{diet}$, f_{C4}, and estimated $\delta^{18}O$ values for cellulose from C_3 and C_4 plants; calculate $\delta^{18}O_{foliarH2O}$ using equation (8); result derived from $\delta^{13}C_{calcite}$	‰

preference for C_3 plants (e.g., leafy plants better adapted to cooler and/or wetter climates), but they generally sample the ambient vegetation in correspondence with the abundance of available plant groups (Milton et al., 1994; Williams et al., 1993). $\delta^{13}C$ values in OES from controlled feeding experiments from South African wild ostriches were shown to reflect dietary (plant) $\delta^{13}C$ values offset by biological fractionation (i.e., the trophic effect; Ambrose and DeNiro, 1986; DeNiro and Epstein, 1981; Vogel, 1983) in both the calcite and total organic fraction (TOF) of the eggshell:

$$\Delta^{13}C_{calcite-diet} = \delta^{13}C_{calcite} - \delta^{13}C_{diet} = +16.2 \pm 0.5‰ \quad (1)$$

and

$$\Delta^{13}C_{TOF-diet} = \delta^{13}C_{TOF} - \delta^{13}C_{diet} = +1.5 \pm 0.8‰ \quad (2)$$

(Johnson et al., 1998; Von Schirnding et al., 1982). The $\delta^{13}C_{diet}$ of ostriches and inferred local vegetation can be calculated from either empirical relationship for the calcite or TOF $\delta^{13}C$ values. In modern OES, the difference between the $\delta^{13}C$ values of eggshell calcite and TOF reflect a constant biological fractionation $\Delta^{13}C_{calcite-TOF} = 14.7‰$ (Johnson et al., 1998). While one study has shown that in Japanese quail bone, the sources of bone carbon have different time dependences (Hobson and Clark, 1992), Johnson et al. (1998) demonstrate the consistent $\Delta^{13}C_{calcite-TOF}$ in OES of wild foraging ostriches whose shells derive from a ~5 year sampling interval. This $\Delta^{13}C_{calcite-TOF}$ relation should also apply in well-preserved ancient eggshells and is a necessary condition for inferring that primary C and N isotope values have been retained by ancient OES. Accordingly, Johnson et al. (1998) recommended a widely accepted criterion of:

$$\Delta^{13}C_{calcite-TOF} = 15 \pm 2‰ \quad (3)$$

2.1.2. Nitrogen isotopes in ostrich eggshell

Ostriches obtain nitrogen primarily from consumed green plant material (i.e., leaves), so the $\delta^{15}N$ values of OES are higher relative to foliar $\delta^{15}N$ values due to the trophic effect (Ambrose and DeNiro, 1986; DeNiro and Epstein, 1981). Plants take up nitrogen from the soil with negligible fractionation, especially in N-limited systems frequently found in semi-arid to arid climates (Högberg, 1997). Therefore, OES foliar $\delta^{15}N$ values should mainly reflect the N isotopic composition of soil sources. Soil $\delta^{15}N$ values increase with decreasing MAP (Amundson et al., 2003) due to water availability effects on soil N dynamics and belowground trophic effects (Högberg, 1997). Previous work has demonstrated strong inverse linear relationships between foliar $\delta^{15}N$ values and MAP (e.g., Austin and Sala, 1999; Craine et al., 2009). Because ostriches derive their nitrogen from leaves, OES $\delta^{15}N$ values should preserve this inverse relationship with MAP (e.g., Johnson et al., 1998). This should record rainfall from the most recent rainy season when leaves grew last, with some time-averaged component depending on the timescales and proportion of N storage in a plant. Most areas inhabited by ostriches experience seasonal long rains rather than year-round rainfall (i.e., a winter or summer rainfall season); hence, most rain for the year occurs in the season preceding egg-laying. Therefore, OES $\delta^{15}N$ values from seasonally laid eggs should closely reflect MAP, or perhaps slightly underestimate it, if there is a second short rainy season not represented in seasonal egg-laying patterns.

2.1.3. Oxygen isotopes in ostrich eggshell

In well-constrained cases, oxygen isotopes of biomineral carbonates can serve as proxies for aridity, as is the case with tooth enamel carbonate from evaporation-sensitive fauna (Levin et al., 2006), and the ^{17}O composition of eggshell and teeth (Passey et al., 2014). Similarly, Miller and Fogel (2016) have proposed a quantitative aridity proxy using $\delta^{18}O$ values of emu (*Dromaius novaehollandiae*) eggshell, considering that emus are obligate drinkers and their $\delta^{18}O$ values will mainly record the $\delta^{18}O$ values of evaporatively enriched standing water bodies. Other studies have interpreted $\delta^{18}O$ values of OES as a qualitative monitor of changing aridity (Lee-Thorp and Ecker, 2015; Roberts et al., 2016).

2.1.4. Preservation of primary stable isotope compositions

Preservation of primary eggshell composition is required to interpret stable isotope records from ancient OES, and because ostrich eggshell is composed almost entirely of low-Mg calcite, it is stable in soil environments in semi-arid to arid climates. Organics represent ~1–3 wt% of OES comprised mainly of proteins (70%) and polysaccharides (30%) which vary compositionally throughout the eggshell (Feng et al., 2001; Mikhailov, 1997; Nys et al., 1999, and references therein; Von Schirnding et al., 1982). Ratite eggshell calcite structures may be preserved for ~10^6 years, including primary isotopic $\delta^{13}C$ values, under appropriate environmental conditions (e.g., Segalen et al., 2002; Ségalen and Lee-Thorp, 2009; Stern et al., 1994). Amino acids racemize over this timescale and serve as the basis for amino acid racemization (AAR) dating, and because they are sensitive to temperature, the preservation of primary, diagenetically unaltered organic material is on the order of ~10^5–10^6 years in warmer climates (for soil temperatures ~18–26 °C: Brooks et al., 1990). OES from Equus Cave (South Africa) retained the expected $\Delta^{13}C_{calcite-TOF}$ for up to 17 ka (Johnson et al., 1997), and Newsome et al. (2011) presented $\delta^{15}N$ values of eggshells from eggshells of emu and the extinct *Genyornis newtonii* as old as ~130 ka. Because OES are stable under modern storage conditions, archival materials are suitable for light stable isotope analyses and geochronology. While isotopic analyses of animal dentitions (and more rarely bones) found at archaeological or paleontological sites may be used to reconstruct past environments, OES offer an important advantage over these systems in tropical to sub-tropical environments because they can be directly dated by AMS ^{14}C, AAR, and $^{230}Th/U$ burial dating (Bird et al., 2003; Brooks et al., 1990; Niespolo et al., 2018; Sharp et al., 2016, 2019). If additional processes such as burning (altering the isotopic composition of TOF, e.g., Miller et al., 2016) or deposition under unsuitable conditions for calcite stability have altered the eggshell composition, $\Delta^{13}C_{calcite-TOF}$ would fall outside of its natural variability and these samples would not be suitable to interpret the isotopic composition of TOF.

2.1.5. Modern local environmental context

The archaeological sites at Lukenya Hill and Kisese II are separated by only by ~300 m elevation, 3° latitude, and 350 km distance. Yet, the two localities are characterized today by different local ecosystems and rainfall amounts but similar temperatures. Situated on the high plains above the Athi-Kapiti Plain east of the Kenyan Rift Valley at ~1750 mASL, Lukenya Hill has a modern mean annual temperature (MAT) of ~20–24 °C and MAP of ~630 mm/year (McSweeney et al., 2010, 2012b). Vegetation surrounding Lukenya Hill includes edaphic-wooded to upland acacia-wooded grassland (van Breugel et al., 2015). Kisese II is located at ~1460 mASL, ~200 m below the escarpment of the Irangi Hills that form the eastermost margin of the Gregory Rift valley in Tanzania, with a modern MAT of ~21–23 °C and MAP of ~850-1020 mm/year (McSweeney et al., 2010, 2012a; Tryon et al., 2018). Woodlands in the Irangi Hills, wooded and edaphic grasslands at the base of the escarpment, and dry bushland further east, surround Kisese II (van Breugel et al.,

2015), and the site lies at the margin of the *miombo* woodlands characteristic of south-central Africa.

The persistence of grazer-dominated faunas from GvJm 22 (Lukenya Hill) suggests that the MSA/LSA transition occurred despite minimal changes in the local environment (Marean, 1992; Tryon et al., 2015; Robinson, 2017), whereas fauna from Kisese II suggest more diverse ecosystems (Tryon et al., 2019). In other studies, these localities have been determined to straddle a climatic boundary between regions defined as "show[ing] persistent climatic similarities through time" by Blome et al. (2012) (Fig. 1). However, these regions are not populated by equally rich paleoclimate data sets. Kisese II is found within the "tropical Africa" region defined in Blome et al. (2012), a region that is populated by 19 terrestrial paleoclimate records and 5 marine records. Lukenya Hill is found within the "eastern Africa" region defined by Blome et al. (2012), populated by only 3 terrestrial paleoclimate records and no marine records. Hence, OES stable isotope records additionally provide an opportunity to fill gaps in terrestrial records in undersampled regions, such as in eastern Africa.

3. Methods

3.1. Eggshell samples

The majority of the Lukenya Hill (1° 28′ 12.00″S, 37° 0′ 0.00″E) samples came from site GvJm 22, and two came from site GvJm 16 (~500 m from GvJm 22), two of many rockshelter sites on an inselberg of Precambrian gneiss east of the Kenyan Rift Valley (Gramly, 1976; Tryon et al., 2015). All samples were drawn from collections stored at the National Museums of Kenya, Nairobi. Radiocarbon (^{14}C)-dated OES and other lines of evidence indicate that the Lukenya Hill localities record human activities from >46 ka until the early 20th century (Gramly, 1976; Tryon et al., 2015). At site GvJm 22, the MSA/LSA transition has been conservatively estimated between ~46 and 26 ka. This relatively low temporal resolution is a result of the ~50 ka ^{14}C limit, the relatively coarse excavation methods used in the 1970's, and one or more sedimentary unconformities. The MSA/LSA transition is recognized here by a shift from Levallois to blade and bladelet lithic production, the more frequent use of grinding stones, and the increased use of ostrich eggshell beads (Tryon et al., 2015). There is a partial human calvaria (KNM-LH-1) dated to ~23 ka (Tryon et al., 2015). OES beads, fragments, or worked pieces are relatively rare at site GvJm 22 ($n = 16$). Unworked OES fragments from Lukenya Hill were selected for dating and isotopic analysis.

Kisese II is a painted rockshelter among the UNESCO World Heritage Kondoa Rock-Art Sites (4° 25′ 15.00″S, 35° 50′ 0.00″E; Bwasiri and Smith, 2015; Inskeep, 1962; Tryon et al., 2019, 2018). Excavated in 1956, it contains artifacts representative of the MSA/LSA transition including OES beads, ochre, blades, and backed points, as well as much younger red-and-white paintings of humans, animals and geometric figures (Bwasiri and Smith, 2015; Tryon et al., 2018). Twenty-five AMS ^{14}C dates and four conventional ^{14}C dates of OES allowed each horizontally excavated level (or "spit") to be constrained with maximum and minimum ages; the site ranges in age from >46 to 4 ka, with the MSA/LSA transition estimated to have begun ~36–34 ka (Tryon et al., 2018). Kisese II preserves >5000 complete OES beads or fragments (Tryon et al., 2018); the OES studied here are mostly unworked fragments and some partial bead blanks (Fig. 2) from the archived collections stored at the National Museum of Tanzania.

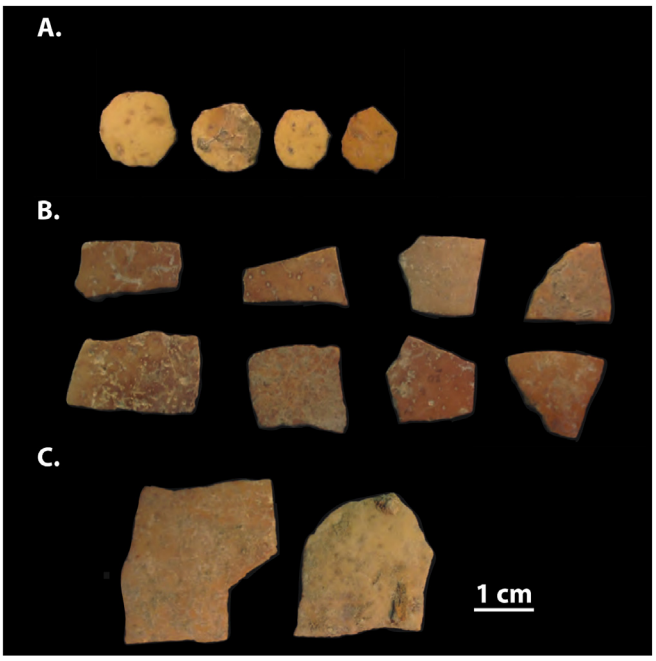

Fig. 2. Selected ostrich eggshell fragments from Kisese II. A. Bead blanks from Spit VI; B. fragments from Spit X; C. fragments from Spit XIII. The 1-cm scale bar applies to each sample.

3.2. Stable isotopes

OES samples were prepared for stable isotope analyses with a novel protocol designed to optimize yields of TOF and obtain reproducible results on fragments from the same eggshell (see Supplementary Materials, Sections 2 and 3; Niespolo et al., 2015). Preliminary testing on 15 fragments from the same farmed modern ostrich eggshell (Solvang, CA) were performed to identify the best acid strength and acidification sequence to use. The protocol requires sample sizes of ~300 mg to completely dissolve the calcite fraction and retain sufficient TOF for online analysis. Further discussion of our findings and complete protocol is presented in the Supplementary Materials (Sections 2 & 3). The N and C isotopic compositions of our modern OES fragments should be similar given that they all derive from the same egg. We measured an average δ^{15}N value = 7.0 ± 0.5‰ and average δ^{13}C. = −24.0 ± 0.4‰ ($n = 11$; Supplementary Table 2). Thus, ancient OES stable isotope compositions should be reproducible at these levels of precision if multiple fragments came from the same egg. Eggs deriving from different ostriches from a number of different years should show greater variation due to differing plants on the landscape, compared to the highly reproducible results of multiple fragments from the same egg.

The stable isotope abundances are reported in delta (δ) notation in parts per thousand (‰) where: $\delta = (R_A/R_S) - 1)$, and R_A and R_S are the ratios of the rare to abundant isotope (^{18}O/^{16}O, ^{15}N/^{14}N, or ^{13}C/^{12}C) in the sample of interest and in an international standard, respectively. Isotopic analyses were completed in the UC Berkeley Center for Stable Isotope Biogeochemistry (CA, U.S.A.). δ^{13}C and δ^{18}O values of the extracted calcite fraction of OES were analyzed using an IsoPrime-DI-MultiPrep system to dissolve samples in H_3PO_4 at 90 °C, in line with a GV IsoPrime mass spectrometer in dual inlet mode. Three internal laboratory standards and an

international standard were used for calibration and/or quality control. These laboratory reference materials are calibrated annually against IAEA (International Atomic Energy Agency, Vienna, Austria) certified reference materials. Calcite $\delta^{13}C$ values are calibrated relative to international standard NBS 19 (limestone) and reported relative to the international standard Vienna Pee Dee Belemnite (VPDB; Hut, 1987). Calcite $\delta^{18}O$ values are reported according to Vienna Standard Mean Ocean Water (VSMOW; Coplen, 1996). Run precision for Lukenya Hill samples based on within-run reproducibility of the quality control standard were 0.019‰ and 0.036‰ for $\delta^{13}C$ and $\delta^{18}O$ values, respectively (Table 2); all errors 1σ). Kisese II samples are reported according to the within-run precision of 0.026‰ for $\delta^{13}C$ and 0.06‰ for $\delta^{18}O$ (samples not labeled from 2017), and 0.05–0.1‰ for $\delta^{13}C$ and 0.046–0.057‰ for $\delta^{18}O$ (samples labeled from 2017; Table 3). Long-term precisions of $\delta^{13}C$ and $\delta^{18}O$ values are respectively 0.05‰ and 0.07‰.

The total organic fraction (TOF) of OES was analyzed using a CHNOS Elemental Analyzer interfaced to an IsoPrime 100 mass spectrometer. Raw data were calibrated using standards NIST (National Institute of Standards and Technology, Gaithersburg, MD, USA) Standard Reference Material (SRM) 1577b (bovine liver) and SRM 1547 (peach). The international standards (relative to which the TOF delta values are reported) are atmospheric nitrogen (air) for $\delta^{15}N$ values and VPDB for $\delta^{13}C$ values. Raw instrument data were corrected for drift over time and linearity and normalized to the international stable isotope reference scale. Run precision is ±0.1‰ and ±0.2‰ for $\delta^{13}C$ and $\delta^{15}N$, respectively, except where specified otherwise in the supplementary data. Long-term external precision is ±0.10‰ and ±0.15‰, respectively for C and N isotope analyses. For both calcite and TOF analyses, standards were added throughout the run for raw data corrections and to measure accuracy and precision. Statistical analyses on data sets were performed in R (R Core Team, 2018).

3.3. Chronology and age modeling

OES from Lukenya Hill and Kisese II come from legacy collections from excavations conducted in the 1950s–1970s (cf. Gramly, 1976; Inskeep, 1962; Tryon et al., 2019, 2018, 2015) that used horizontal excavation units cross-cutting dipping sedimentary deposits. This resulted in the admixture of formerly discrete depositional units, which combined with limited data on the horizontal distribution of material at each site, reduces the resolution of our understanding of the archaeological record.

However, each OES analyzed from Lukenya Hill has been ^{14}C-dated to obviate any ambiguity of chronostratigraphic placement (Tryon et al., 2015), including two unpublished dates on OES from GvJm 16 (Table 2). Samples weighing ~30–50 mg from GvJm 16 were prepared for analysis of the calcite fraction for ^{14}C starting with chemical abrasion of 25% of the sample to avoid surficial modern carbon contamination, as is conventional for ^{14}C dating of ratite eggshells (Bird et al., 2003; Janz et al., 2009). Samples are rinsed in de-ionized water and then hydrolyzed with phosphoric acid (H_3PO_4) in an Exetainer septa seal vial on a heating block at 90 °C to evolve carbon dioxide as described in Santos et al. (2004). AMS ^{14}C analyses were conducted at the Chrono Lab at Queen's University (Belfast, Northern Ireland). For consistency, we report the ^{14}C dates for OES from Lukenya Hill (Table 2) using a mixed southern- and northern hemisphere calibration curve (Hogg et al., 2013; Reimer et al., 2013) to accommodate the samples being from near-equatorial regions. (after Tryon et al. (2018) and using the OxCal software version 4.3; Bronk-Ramsey, 2001; Bronk Ramsey, 2016). Sample 140–150A is calibrated after Cheng et al. (2018) because it is older than the limit of ^{14}C calibrations available in OxCal; for explanation, see Sharp et al. (2019). Seven of the OES from GvJm 22 also have reliable $^{230}Th/U$ burial ages (Sharp et al., 2016, 2019). Therefore, each OES from Lukenya Hill has a stable isotope composition that can be precisely placed in time. At Kisese

Table 2
Lukenya Hill isotope data and re-calibrated ^{14}C ages (after Tryon et al., 2015). All ages but one (140–150A) were calibrated using a mixed calibration between southern and northern hemisphere calibrations (SHCal and IntCal13; Hogg et al., 2013; Reimer et al., 2013), determined using the OxCal software (Bronk-Ramsey, 2001, 2016). Italicized samples have uncertainty of ±0.4‰ on $\delta^{15}N$ rather than usual ±0.2‰. Empty cells indicate samples were too small or not analyzed. Lines separate groups of samples averaged to evaluate mean and standard deviation of a number of OES over discrete time intervals defined by the OES ^{14}C ages. Samples with an asterisk (*) came from GvJm16, a nearby rock shelter sequence, and these dates are presented here for the first time.

Lukenya Hill Sample ID	Trench	Total Organic Fraction				Calcite Fraction		$\Delta^{13}C_{Calcite-TOF}$ (‰)	Geochronology	
		% N	$\delta^{15}N$ (AIR, ‰)	% C	$\delta^{13}C_{org}$ (VPDB, ‰)	$\delta^{13}C_{calcite}$ (VPDB, ‰)	$\delta^{18}O$ (VSMOW, ‰)		^{14}C Lab ID	calBP (95.4%)
110–120	A	8.65	6.3	43.81	−22.4	−7.39	34.02	15.0	UBA-24889	3867–3693
120–130A	B	12.93	5.4	48.03	−22.0	−7.25	35.49	14.8	UBA-24877	4814–4444
160–170	B	4.10	*4.5*	43.40	−22.5	−6.25	35.96	16.2	UBA-24887	4782–4416
150–160	B	11.12	7.1	42.10	−21.0	−6.07	34.74	15.0	UBA-24879	4861–4630
120–130A	Test Pit					−7.84	35.16		UBA-23927	5276–4871
105–110	C	9.41	7.3	37.95	−16.0	−3.20	34.70	12.8	UBA-24888	6879–6669
98.50–98.45A*	Test Pit	8.71	6.6	36.07	−22.5	−6.85	37.54	15.6	UBA-24894	12,703–12,178
98.45–98.40B*	Test Pit	7.43	*5.7*	38.90	−23.0	−9.51	29.09	13.5	UBA-24893	13,710–13,403
120–130B	A	4.61	9.7	48.62	−22.2	−7.37	37.85	14.8	UBA-24885	15,350–14,933
120–130C	A	7.14	9.3	58.31	−22.2	−7.37	38.89	14.8	UBA-24886	15,565–15,119
130–140A	Test Pit					−1.59	39.97		UBA-23928	15,591–15,157
140–150A	A	6.09	*8.9*	49.82	−23.1	−6.68	37.05	16.4	UBA-24881	15,691–15,239
120–130A	A	4.33	8.4	34.04	−22.5	−4.69	37.33	17.8	UBA-24884	15,771–15,283
140–150C	A	10.04	9.2	49.62	−21.9	−6.49	38.49	15.4	UBA-24883	18,830–18,422
140–150B	A	5.37	*9.0*	53.63	−23.0	−6.40	36.19	16.6	UBA-24882	22,155–21,565
140–150B	Test Pit			44.52	−24.4	−4.04	36.66		UBA-23933	23,888–23,180
130–140C	Test Pit	6.97	8.0	54.27	−22.8	−4.12	36.56	18.7	UBA-23930	23,924–23,226
130–140B	Test Pit	5.34	9.2	49.32	−23.1	−4.15	36.28	18.9	UBA-23929	23,996–23,355
190-Breccia	A	7.22	7.8	36.05	−20.7	−3.12	36.07	17.6	UBA-24890	26,319–25,777
170–180	B	5.40	*8.8*	38.99	−23.0	−7.26	34.29	15.8	UBA-24878	32,583–31,194
140–150C	Test Pit	6.70	10.8	48.34	−21.4	−5.03	37.27	16.4	UBA-23934; AA 102890	32,792–31,247
130–140A	B	4.07	*10.3*	28.49	−20.8	−4.07	34.34	16.8	UBA-24880	38,498–35,974
140-150D	Test Pit	8.14	11.1	49.94	−22.2	−7.12	34.78	15.1	UBA-23935; AA102889	39,002–36,103
140–150A	Test Pit	3.32	10.0	42.28	−21.9	−3.46	36.35	18.4	UBA-23932	50,003–45,201

Table 3
Isotope data for Kisese II. Italicized samples have 1σ analytical precision $\delta^{13}C_{calcite}$ = 0.1‰ analytical precision, $\delta^{18}O_{calcite}$ = 0.057‰; all others are $\delta^{13}C_{calcite}$ = 0.05‰ and $\delta^{18}O_{calcite}$ = 0.046‰. Ages and age ranges are after Tryon et al. (2018).

Kisese II Sample ID	Spit	Total Organic Fraction				Calcite Fraction		$\Delta^{13}C_{Calcite\text{-}TOF}$ (‰)	Geochronology			
		% N	$\delta^{15}N$ (AIR, ‰)	% C	$\delta^{13}C$ (VPDB, ‰)	$\delta^{13}C$ (‰ VPDB)	$\delta^{18}O$ (‰, VSMOW)		UBA-No.	calBP (95.4%)	maximum age (ka)	minimum age (ka)
KII II-B	II					−7.77	35.13		UBA-27430	4230–3990	4.23	3.99
KII I–B	I	1.97	6.8	7.26	−20.0	−4.57	36.60	15.42	UBA-27428	4380–4090	4.38	4.09
2017KII-I-A	I	14.19	7.4	50.22	−19.3	*−4.49*	34.36	14.83			4.4	4.1
2017KII-I-B	I	14.15	7.0	50.90	−22.5	*−9.13*	*31.11*	13.34			4.4	4.1
2017KII-Ib-A	Ib	13.01	8.0	52.86	−22.1	*−8.38*	*30.90*	13.67			4.4	4.1
KII I-A	I	9.04	6.4	31.72	−19.1	−4.87	34.76	14.22	UBA-27427	4410–4160	4.41	4.16
KII V–B	V	8.66	5.9	35.35	−22.7	−9.66	33.33	13.00	UBA-27434	10,650 –10,300	10.65	10.3
2017KII-II-A	II	13.21	6.6	51.00	−20.9	*−7.30*	*29.60*	13.56			18.1	4.2
2017KII-II-B	II	10.06	8.0	55.97	−22.8	*−9.04*	*29.28*	13.80			18.1	4.2
2017KII-II-C	II	9.06	5.7	58.91	−24.1	*−8.77*	*32.83*	15.37			18.1	4.2
KII III-B	III	5.89	9.2	24.27	−19.0	−4.01	35.51	15.00	UBA-27432	17,230 –16,720	17.23	16.72
2017KII-III-A	III	13.05	6.9	50.15	−21.9	*−7.67*	*32.53*	14.27			17.5	16.7
2017KII-III-B	III	9.47	4.9	52.16	−23.3	*−8.55*	*30.63*	14.71			17.5	16.7
KII III-A	III	1.91	7.5	9.20	−22.2	−6.01	34.84	16.22	UBA-27431	17,550 –17,140	17.55	17.14
2017KII-IV-B	IV	9.63		48.14	−22.7	*−8.36*	*33.31*	14.35			18.4	17.4
2017KII-IV-A	IV	10.82	11.1	48.18	−21.7	*−9.72*	*34.38*	11.99			18.4	17.4
KII II-A	II	5.91	7.1	41.22	−22.7	−6.13	34.59	16.55	UBA-27429	18,190 –17,840	18.19	17.84
2017KII-V-A	V	12.91	6.1	52.63	−21.2	*−8.72*	*33.86*	12.46	UBA-34477	18,250 –17,900	18.25	17.9
2017KII-V-B	V	8.69	3.4	51.39	−24.1	*−8.73*	*30.95*	15.33			18.8	17.9
2017KII-V-C	V	11.89	8.9	49.09	−21.1	*−7.39*	*34.80*	13.75			18.8	17.9
KII V-A	V	9.30	8.3	36.84	−15.1	−0.63	34.89	14.46	UBA-27433	18,810 –18,510	18.81	18.51
KII XXI-A	XXI	4.08	7.9	17.65	−22.2	−7.26	36.91	14.93	UBA-27441	19,230 –18,890	19.23	18.89
2017KII-VI-A	VI	13.05	5.4	52.18	−21.6	*−8.00*	*31.72*	13.60			22.7	17.9
2017KII-VI-B	VI	11.15	7.6	51.17	−17.5	*−2.28*	*33.89*	15.22			22.7	17.9
2017KII-VI-C	VI	10.57	6.5	43.12	−20.6	*−3.55*	*34.69*	17.03			22.7	17.9
2017KII-VI-D	VI	11.27	8.6	50.82	−16.6	*−1.82*	*31.71*	14.76			22.7	17.9
2017KII-VII-B	VII	9.66	7.3	53.86	−19.7	*−3.18*	*34.49*	16.51			22.7	17.9
2017KII-VII-C	VII	7.38	7.4	63.44	−21.8	−7.05	33.08	14.79			22.7	17.9
2017KII-VIII-A	VIII	12.22	6.0	50.76	−21.3	−5.87	36.53	15.42			22.7	17.9
2017KII-VIII-B	VIII	12.27	7.4	52.06	−21.4	−7.57	33.03	13.83			22.7	17.9
2017KII-VIII-C	VIII	11.08	6.7	48.23	−21.5	−7.07	35.29	14.44			22.7	17.9
2017KII-VIII-D	VIII	12.23	7.3	49.16	−17.9	−2.35	38.24	15.58			22.7	17.9
2017KII-IX-A	IX	10.60	8.1	43.70	−19.6	−4.60	33.97	15.02			22.7	21.2
2017KII-IX-B	IX	6.44	6.7	35.16	−22.6	−6.20	37.41	16.39			22.7	21.2
2017KII-IX-C	IX	8.65	4.9	58.94	−21.9	−6.53	36.75	15.39			22.7	21.2
2017KII-IX-D	IX	3.20	5.7	13.04	−18.5	−6.95	35.99	11.54			22.7	21.2
2017KII-X-B	X	3.99	4.8	30.63	−22.5	−5.53	36.95	16.97			23.7	23.1
2017KII-X-C	X	9.63	5.1	61.02	−22.7	−8.14	36.56	14.52			23.7	23.1
2017KII-X-D	X	7.33	5.7	54.11	−23.5	−8.26	34.09	15.21			23.7	23.1
2017KII-X-E	X	6.89	4.3	42.07	−24.2	−8.52	33.95	15.70			23.7	23.1
2017KII-X-F	X	7.38	7.0	28.55	−19.4	−7.20	33.27	12.24			23.7	23.1
2017KII-X-G	X	9.59	8.1	60.41	−22.6	−8.44	35.46	14.14			23.7	23.1
2017KII-X-H	X	6.41	7.4	37.83	−22.6	−6.52	35.75	16.04			23.7	23.1
2017KII-X-A	X	5.99	5.3	38.43	−23.3	−7.59	36.50	15.69	UBA-34479	23,680 –23,130	23.68	23.21
KII XII-B	XII	5.55	6.6	23.53	−21.8	−7.25	35.43	14.53	UBA-27436	34,580 –33,720	34.58	33.72
2017KII-XII-A	XII	9.62	5.2	42.47	−22.0	−7.65	35.17	14.36			35.1	33.7
2017KII-XII-B	XII	8.74	6.0	43.48	−23.2	−9.83	33.66	13.39			35.1	33.7
KII XII-A	XII	7.34	6.8	33.76	−23.0	−9.45	34.62	13.53	UBA-27435	35,050 –34,050	35.05	34.05
2017KII-XI-A	XI	6.67	6.1	42.95	−21.7	−7.45	34.37	14.25	UBA-34480	35,140 –34,250	35.1	34.3
2017KII-XI-B	XI	7.43	6.3	32.52	−18.6	−3.55	35.65	15.03			35.1	34.3
2017KII-XI-D	XI	5.73	4.8	43.20	−20.4	−4.00	35.28	16.44			35.1	34.3
2017KII-XI-F	XI	10.55	7.1	52.21	−17.1	−2.37	32.30	14.73			35.1	34.3
2017KII-XI-G	XI	9.07	5.9	41.60	−19.7	−5.32	33.85	14.42			35.1	34.3
2017KII-XI-H	XI	11.43	5.9	58.02	−22.2	−9.50	32.60	12.73			35.1	34.3
2017KII-XI-C	XI	7.19	7.5	68.55	−23.0	−6.84	35.65	16.18			35.1	34.3
2017KII-XI-E	XI	8.92	5.6	37.53	−21.7	−7.30	35.76	14.41			35.1	34.3

(*continued on next page*)

Table 3 (*continued*)

Kisese II Sample ID	Spit	Total Organic Fraction				Calcite Fraction		$\Delta^{13}C_{Calcite\text{-}TOF}$ (‰)	Geochronology			
		% N	$\delta^{15}N$ (AIR, ‰)	% C	$\delta^{13}C$ (VPDB, ‰)	$\delta^{13}C$ (‰ VPDB)	$\delta^{18}O$ (‰, VSMOW)		UBA-No.	calBP (95.4%)	maximum age (ka)	minimum age (ka)
KII XV-A	XV	3.29	7.2	19.42	−21.5	−5.91	33.07	15.55	UBA-27437	35,470 −34,270	35.47	34.27
2017KII-XV-A	XV	2.81	6.9	13.17	−19.8	−9.85	30.77	9.98			35.9	34.3
2017KII-XV-B	XV	3.62	6.3	16.68	−21.8	−6.82	31.98	15.00			35.9	34.3
KII XV-B	XV	3.42	4.3	18.75	−22.6	−7.78	34.89	14.82	UBA-27438	35,850 −34,660	35.85	34.66
2017KII-XIV-D	XIV	1.65		5.62	−22.5	−5.65	35.08	16.83			39.9	33
2017KII-XIV-A	XIV	3.61	6.0	15.67	−21.3	−7.38	34.99	13.91			39.9	33
2017KII-XIV-B	XIV	2.90	7.6	12.12	−19.5	−8.96	31.28	10.50			39.9	33
2017KII-XIII-A	XIII	1.77	7.3	8.30	−16.9	−3.77	34.13	13.08			39.9	33.7
2017KII-XIII-B	XIII	3.29	6.3	14.26	−20.7	−7.23	36.69	13.50			39.9	33.7
2017KII-XVI-A	XVI	4.15	8.9	18.46	−20.9	−5.84	34.30	15.03			39.6	34.3
2017KII-XVI-B	XVI	2.33	6.5	16.68	−21.1	−6.48	34.14	14.66			39.6	34.3
2017KII-XVII-A	XVII	1.08	7.5	5.02	−18.8	−7.04	32.39	11.73			39.6	34.3
2017KII-XVII-B	XVII	2.00	8.6	9.51	−17.4	−2.66	35.15	14.69			39.6	34.3
2017KII-XVII-C	XVII	1.51	6.8	10.33	−16.5	−4.84	33.31	11.70			39.6	34.3
KII XIX-A	XIX	1.89	6.2	10.32	−22.6	−7.41	32.50	15.19	UBA-27439	38,600 −36,600	38.6	36.6
2017KII-XVIII-B	XVIII	4.24	6.2	19.18	−21.9	−5.56	39.65	16.31	UBA-34481	39,590 −38,340	39.6	38.3
2017KII-VII-A	VII	9.04	11.4	49.17	−19.4	*−6.90*	*32.77*	12.49	UBA-34478	42,790 −41,730	42.79	41.73
2017KII-XX-B	XX	2.04	8.3	18.72	−22.1	−8.20	28.76	13.92			46.2	42.7
2017KII-XX-C	XX	2.59	8.7	20.87	−23.1	−7.87	30.11	15.23			46.2	42.7
2017KII-XX-D	XX	1.11	9.0	6.98	−18.6	−3.90	33.93	14.74			46.2	42.7
2017KII-XX-E	XX	1.95	6.1	15.42	−22.6	−6.18	32.98	16.47			46.2	42.7
2017KII-XX-F	XX	1.05	7.2	7.25	−22.1						46.2	42.7
2017KII-XXI-B	XXI	1.78	9.4	15.48	−19.9	−2.68	37.16	17.17			46.8	42.7
2017KII-XXI-C	XXI	1.68	6.6	13.50	−22.0						46.8	42.7
2017KII-XXI-D	XXI	1.39	8.9	12.22	−20.2	−7.03	32.85	13.15			46.8	42.7
KII XIX-B	XIX	4.03	6.4	25.71	−21.2	−4.93	32.02	16.29	UBA-27440	46,710 −42,990	46.71	42.99
KII XXI-B	XXI	3.94	6.2	27.34	−20.9	−5.69	33.18	15.25	UBA-27442	46,850 −43,120	46.85	43.12

II, 29 OES were ^{14}C-dated to estimate age ranges for each horizontally excavated unit (Tryon et al., 2018) and are reported in Table 3 using the same mixed calibration curve. It was impractical to date every OES from Kisese II ($n = 87$); therefore, the ages of some OES fragments not directly ^{14}C-dated are bounded by the age range of the excavated spit that contained them as given in Tryon et al. (2018) and provided in Table 3. All published ^{14}C dates derive from the calcite fraction of the OES.

In an effort to smooth out variation introduced by feeding habits of individual birds and interannual variations in vegetation and rainfall, we evaluate multiple OES per time interval (range of n for $\delta^{15}N = [2, 11]$, median $n = 4$; range of n for $\delta^{13}C$, $\delta^{18}O = [2, 12]$, median $n = 5$) and compare means and standard deviations (σ) of contemporaneous OES isotope proxies between sites. We take the average isotopic compositions of 2–5 OES at Lukenya Hill in groups according to their calibrated ^{14}C ages. At Kisese II, some spits overlap with others in age. We have thus divided these overlapping spits into age ranges that accommodate the highest temporal resolution possible and still include at least 4 OES fragments per binned interval. Even at coarse chronological resolution, mean isotope values in each system overlap at 1σ between groups with overlapping time intervals. However, lacking precise and continuous chronological resolution, more robust statistical methods to integrate stable isotope results through time (such as moving average approaches) were not justifiable and resulted in either truncated, overly smoothed models (for large n in the moving average, or large smoothing parameters) or inaccurate moving average results from integration of temporally disparate data. To visualize how each isotope system changes through time at Kisese II, we use linear interpolation of mean values from age bins for each isotope system, but with expanded uncertainties in intervals with less precise chronology (for example, from 18.1 to 4.2 ka, uncertainties reflect the sum of uncertainties of overlapping bins).

4. Results from ancient OES

We used all samples with both TOF and calcite isotopic data in order to calculate $\Delta^{13}C_{calcite\text{-}TOF}$ (Fig. 3, after equation (3), Johnson et al., 1998). Deviation from the expected $\Delta^{13}C_{calcite\text{-}TOF}$ range was interpreted as alteration of the primary isotopic composition of TOF. Only the calcite isotopic composition of those samples were further evaluated. Twenty-three OES calcite samples were analyzed from Lukenya Hill, 21 of which yielded sufficient material for online analysis of TOF. Fifteen out of 21 OES from Lukenya Hill show the expected $\Delta^{13}C_{calcite\text{-}TOF}$ (Fig. 3) and retain primary TOF isotopic compositions by inference. Eighty-four of 87 samples analyzed from Kisese II were large enough to yield sufficient TOF for analysis; 73 of 84 samples reproduced the expected $\Delta^{13}C_{calcite\text{-}TOF}$ (Fig. 3). There is no apparent relationship between sample age and TOF isotopic preservation (Fig. 4), indicating that age is not a primary control on it and the technique should be applicable on timescales similar to those of preservation of amino acids in eggshells (~10^5–10^6 years; e.g., Brooks et al., 1990; Demarchi et al., 2016). Samples too small to produce sufficient TOF for isotopic analysis were still large enough to produce calcite $\delta^{13}C$ and $\delta^{18}O$ values. All isotope data, and C and N compositions from the TOF of 110 OES fragments collected from the archaeological sites are found in Tables 2 and 3 and all individual OES calculated proxy values can be found in the Supplementary Data. While there are many more OES available at Kisese II compared to Lukenya Hill, these records are

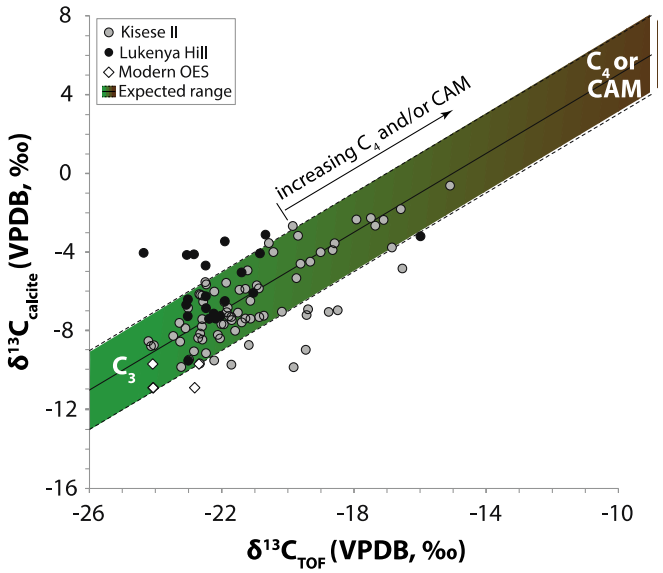

Fig. 3. Plot of $\delta^{13}C$ values of total organic fraction (TOF) versus inorganic fraction (calcite) of modern (Solvang, CA) and ancient ostrich eggshells from this study. Green panel shows expected $\Delta^{13}C_{calcite\text{-}TOF} = 15 \pm 2‰$ (mean: solid line; uncertainty: dashed lines). Boxes show compositions expected for diets consisting of 100% C_3 and 100% C_4 plants; endmember values are discussed in Section 4.1. The endmember for C_4 and/or CAM plants in the diet is referred in the text as the C_4 component of the diet. Solid line with dashed uncertainties (after Johnson et al., 1998) shows the consistent fractionation observed between TOF and calcite in modern eggshells regardless of diet. Ancient eggshells plotting within the dashed lines preserve pristine carbon isotope fractionation, and by inference, primary $\delta^{15}N$ values. (For interpretation of the references to color in this figure legend, the reader is referred to the Web version of this article.)

both constrained in time well enough to allow comparisons between temporally equivalent groups of data. Tables 4 and 5 provide the mean isotopic values for each time interval at Lukenya Hill and Kisese II, respectively, and the inferred mean proxy values for each system. Fig. 5 provides the measured $\delta^{13}C$, $\delta^{15}N$, and $\delta^{18}O$ values, as well as the calculated individual and mean $\delta^{13}C$ values of the ostrich diet, corresponding PMAP, and foliar $\delta^{18}O$ values, as a function of time, at Lukenya Hill. Fig. 6 shows the same information for Kisese II. Below we summarize the results of each isotope system at both sites through time.

4.1. Carbon isotopes

We calculate the proportion of C_3 versus C_4 and/or CAM plants in the diet from the $\delta^{13}C$ values of ancient OES based on a simple two end-member linear mixing model (Fig. 3), taking a global average value for each end-member (average $\delta^{13}C_{C3} = -28.5‰$, Kohn, 2010; $\delta^{13}C_{C4} = -13‰$, e.g., Ehleringer and Cerling, 2002). In a study compiling modern global $\delta^{13}C$ values of C_3 plants, Kohn (2010) suggests there is a maximum $\delta^{13}C = -23‰$ for C_3 plants. We apply a cutoff $\delta^{13}C$ value of plants (and corresponding $\delta^{13}C_{diet}$ value) $= -21.5‰$ to evaluate the presence/absence of C_4 plants on the landscape; this conservatively accounts for a ~1.5‰ decrease in the average $\delta^{13}C$ of atmospheric CO_2 from post-industrial plants sampled by these modern studies due to the Suess Effect (e.g., Farquhar et al., 1989; Keeling, 1979; Keeling et al., 2017). $\delta^{13}C$ values for C_3 plants $> -23‰$ are restricted to places with MAP <10 mm/year and some settings with the genus *Pinus*, which is native only to northern African circum-Mediterranean regions prior to historical introduction to South Africa in the 17th century (e.g., Moran et al., 2000). $\delta^{13}C$ values of select modern eastern African plants range from -27.0 to $-31.4‰$ for C_3 plants and from -11.8 to $-13.1‰$ for C_4 plants (Cerling et al., 2003), in agreement with the mean global values.

Crassulacean acid metabolism (CAM) plants may also be present in these environments and subsequently in ostrich diets (e.g., Williams et al., 1993) but can be difficult to resolve because they are isotopically indistinguishable from C_3 and C_4 plants (Cornwell et al., 2016, 2018; Farquhar et al., 1989). We also cannot infer their presence on the landscape directly since they do not have hard parts (e.g., phytoliths) preserved in the geologic record. However, given there is no evidence in the modern landscape or faunal records that

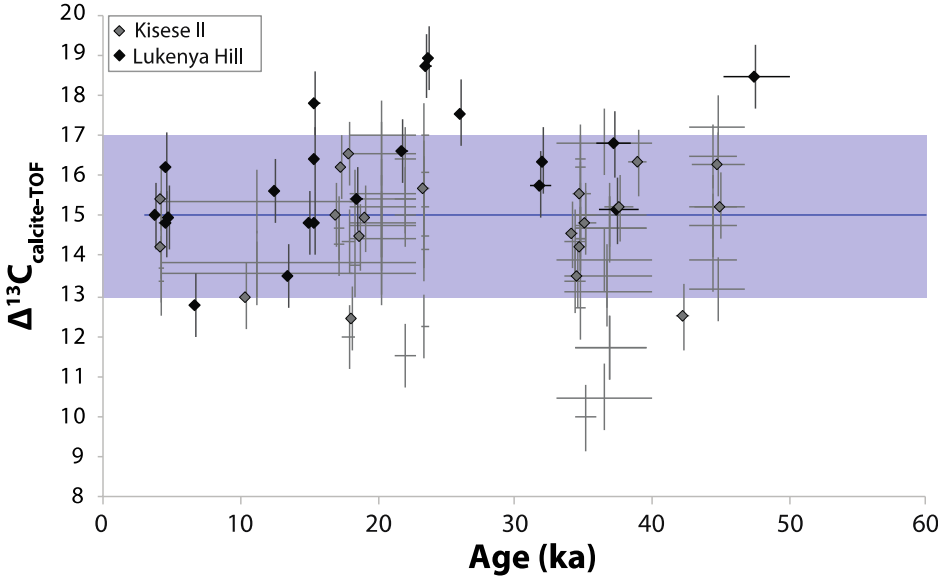

Fig. 4. Carbon isotope fractionation in OES versus age. Pristine $\Delta^{13}C_{calcite\text{-}TOF}$ of $15 \pm 2‰$ is shown by blue line and shaded area, respectively. Most samples show fractionation within the expected range. Those that do not are poorly correlated with age, suggesting diagenesis is controlled by other factors. All Lukenya Hill and some Kisese II eggshells were directly dated via ^{14}C (diamond symbols). Ages of remaining Kisese II samples were estimated from dates on samples in the same excavation level (crosses; length of horizontal bar indicates age range). Ages are from this study and Tryon et al. (2015, 2018). (For interpretation of the references to color in this figure legend, the reader is referred to the Web version of this article.)

Table 4
Mean isotope values and proxies for Lukenya Hill. ^{14}C ages were used to constrain each interval of time represented.

Age range from (ka)	Age range to (ka)	Mean $\delta^{13}C$ (VPDB, ‰)	Mean $\delta^{13}C_{diet}$ (‰)	± (1σ)	Mean $\delta^{15}N$ (AIR, ‰)	± (1σ)	Mean PMAP (mm/yr)	± (1σ)	Mean $\delta^{18}O$ (VSMOW) (‰)	± (1σ)	Model 1 mean $\delta^{18}O_{foliarH2O}$	± (1σ)	Model 2 mean $\delta^{18}O_{foliarH2O}$	± (1σ)	*n*
6.9	3.7	−6.3	−22.5	1.7	5.8	1.1	790	103	35.0	0.7	3.9	0.5	2.0	0.8	4 (N); 4 (C/O)
13.7	12.2	−8.2	−24.4	1.9	6.1	0.6	761	55	34.1	3.6	2.7	4.1	1.1	0.9	2 (N); 5 (C/O)
18.8	14.9	−5.7	−21.9	2.2	9.2	0.3	482	28	38.3	1.1	6.1	0.7	2.4	1.1	5 (N); 7 (C/O)
26.3	21.6	−4.4	−20.6	1.2	ND	ND	ND	ND	36.4	0.2	4.8	0.2	3.0	0.6	4 (C/O)
50.0	31.2	−5.4	−21.6	1.7	10.3	1.0	391	94	35.4	1.3	4.1	0.9	2.5	0.9	3 (N); 5 (C/O)

Table 5
Mean isotope and proxy values through time at Kisese II. Italicized error on PMAP value is an arbitrarily imposed error due to there being only one sample in this interval; errors are standard deviation of the mean value. ^{14}C ages and suggested age ranges after Tryon et al. (2018) were used to constrain each interval of time represented.

Age range from (ka)	Age range to (ka)	Mean $\delta^{13}C$ (VPDB, ‰)	Mean $\delta^{13}C_{diet}$ (‰)	± (1σ)	Mean $\delta^{15}N$ (AIR, ‰)	± (1σ)	Mean PMAP (mm/yr)	± (1σ)	Mean $\delta^{18}O$ (VSMOW) (‰)	± (1σ)	Model 1 mean $\delta^{18}O_{foliarH2O}$	± (1σ)	Model 2 mean $\delta^{18}O_{foliarH2O}$	± (1σ)	*n*
4.4	4.0	−6.5	−22.7	2.1	7.1	0.6	674	54	33.8	2.3	3.0	1.6	1.9	1.1	5
10.7	10.3	−9.7	−25.9	0.9	5.9	0.2	779	*100*	33.3	1.0	2.7	1.0	0.4	1.0	1
18.1	4.2	−8.4	−24.6	0.9	6.8	1.2	705	105	30.6	2.0	0.8	1.3	1.0	0.5	3
17.6	16.7	−6.6	−22.8	2.0	7.1	1.8	671	158	33.4	2.2	2.7	1.5	1.9	1.0	3
19.2	17.4	−7.1	−23.3	2.8	7.1	2.2	674	195	34.2	1.7	3.3	1.2	1.7	1.4	4 N; 6 C/O
22.7	17.9	−4.9	−21.1	2.5	7.0	0.9	681	81	34.3	2.1	3.3	1.4	2.8	1.2	10
22.7	21.2	−6.1	−22.3	1.0	6.6	1.6	723	143	36.0	1.5	4.5	1.0	2.2	0.5	3 N; 4 C/O
23.7	23.1	−7.5	−23.7	1.1	5.8	1.4	788	128	35.3	1.4	4.1	0.9	1.4	0.5	5 N; 8 C/O
35.1	33.7	−6.7	−22.9	2.4	6.2	0.8	758	73	34.5	1.2	3.5	0.8	1.9	1.2	11 N; 12 C/O
35.9	34.3	−7.6	−23.8	1.7	5.9	1.5	779	134	32.7	1.7	2.3	1.2	1.4	0.8	3 N; 4 C/O
39.9	33.0	−6.6	−22.8	2.0	6.5	0.7	729	60	34.4	2.0	3.5	1.4	1.9	1.0	3 N; 75C/O
39.6	34.3	−5.7	−21.9	1.6	7.3	1.3	658	121	34.5	2.5	3.5	1.7	2.4	0.8	5 N; 7 C/O
46.9	41.7	−5.9	−22.1	1.8	7.6	1.3	626	122	32.6	2.4	2.2	1.6	2.2	0.9	7 N; 11 C; 9 O

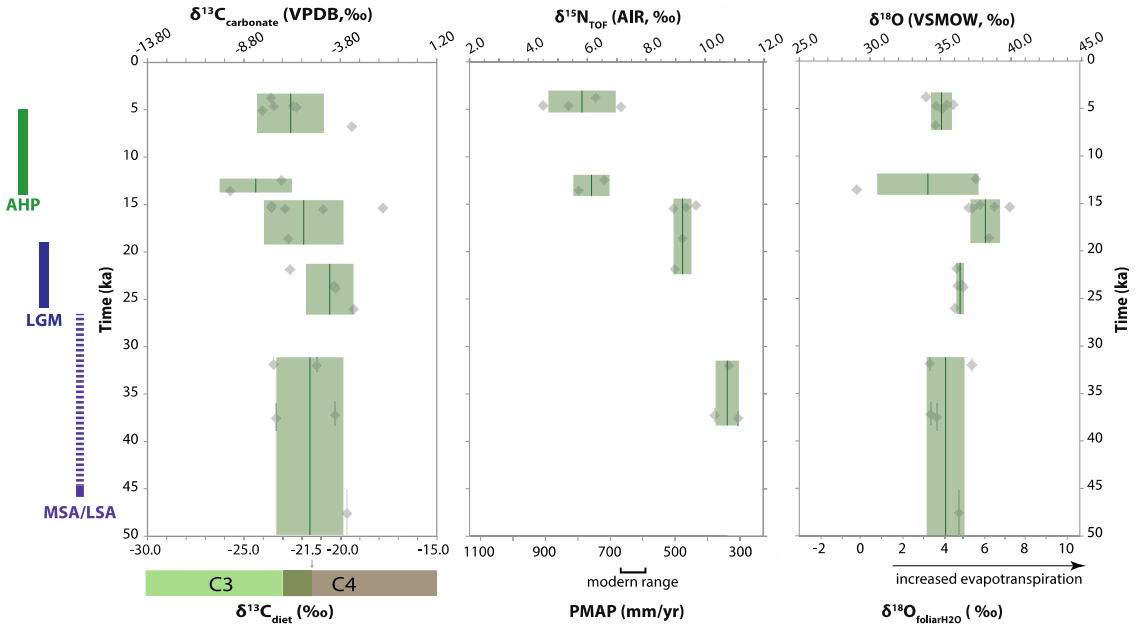

Fig. 5. The C, N, and O isotopic compositions of OES from Lukenya Hill and corresponding proxy variables through time. Each OES from Lukenya Hill was ^{14}C-dated. Green boxes show mean and standard deviation for grouped data. Calculated paleo-mean annual precipitation (PMAP) progressively increases through time from ~38 to 4 ka and correlates with a modest shift toward more C_3-rich diet. The MSA/LSA transition at Lukenya Hill, from c. >46–26 ka, occurs during the period with the lowest inferred mean PMAP in our record. $\delta^{18}O$ values do not co-vary consistently with C and N isotopes.

CAM is/was predominant on the landscape near these localities (Marean, 1992, 1991; Robinson, 2017; Tryon et al., 2019; van Breugel et al., 2015), we will refer to plant dietary $\delta^{13}C$ values that may be isotopically ascribed to C_4 or CAM as the "C_4" endmember.

At Lukenya Hill, calcite $\delta^{13}C$ values range from −1.6‰ to −9.5‰, corresponding to a range of calculated diet $\delta^{13}C$ values varying from −17.8‰ to −25.7‰ (Table 2 and Supplementary Data). These imply ostriches were consuming diverse diets, with between 8 and 60% contributions of C_4 plants (mean = 33 ± 12% C_4 diet). Ten of 23 OES produced dietary $\delta^{13}C$ values greater than −21.5‰, indicating a

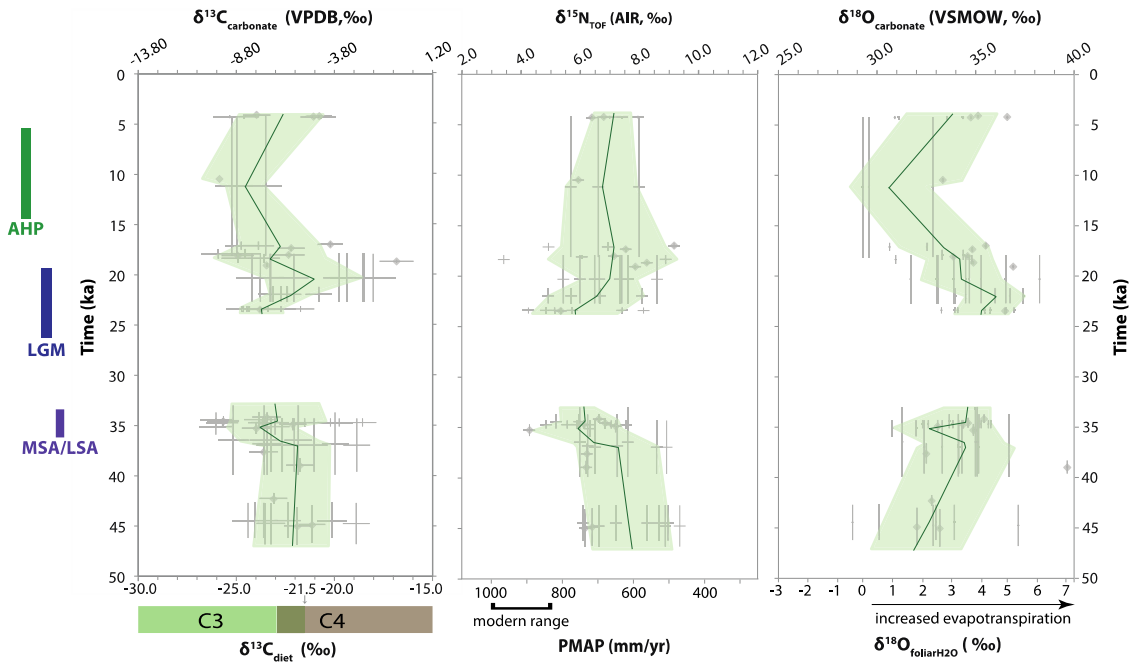

Fig. 6. The C, N, and O isotopic compositions of OES from Kisese II and corresponding proxy variables through time. Grouping of mean values is explained in the text. ^{14}C-dated samples are shown in gray diamonds. Individual analyses (gray crosses) are averaged over discrete time intervals to show trends through time (green lines; green shading shows 1σ envelope around mean). Trends reveal co-occurring shifts in vegetation and precipitation to ~50 ka. Dietary δ^{13}C values (left) trend toward more C_3-rich vegetation during periods with higher rainfall (center panel) and correspond with increased evapotranspiration (right). There are broadly oscillating trends in mean proxy values over time, with peak PMAP occurring at ~22 ka and ~36–34 ka, approximately coincident with the onset of the MSA/LSA transition (36–34 ka) at Kisese II.

C_4-dominant diet in nearly half the samples. Mean dietary δ^{13}C values (Table 4) range from −20.6 ± 1.2‰ to −24.4 ± 2.2‰, indicative of mixed to C_4-rich diets in different time intervals.

At Kisese II, calcite and TOF δ^{13}C values correspond to a range of dietary δ^{13}C values between −16.8‰ and −26.1‰ (Table 3 and Supplementary Data), reflecting 6–66% C_4 dietary contribution (mean C_4 contribution = 28 ± 13.7%), similar to the Lukenya Hill OES samples. Twenty-one of 87 OES produced dietary δ^{13}C values greater than −21.5‰, indicating a C_4-rich diet in fewer than one-quarter of the samples. At Kisese II, mean values of $\delta^{13}C_{diet}$ through time reflect a mixed to C_3-rich diet (Table 5).

4.2. Nitrogen isotopes

The N isotopic composition of eggshell of wild South African ostrich and Australian emu are inversely related to MAP in their native habitats (Johnson et al., 1998; Newsome et al., 2011). Since foliar N is found to be inversely related to MAP globally (Craine et al., 2009), we expect similar relationships between δ^{15}N values of ratite eggshells and MAP to apply wherever ratite feeding habits are similar. Fig. 7 shows that modern eggshell δ^{15}N values of both ratite species from different continents plotted versus contemporary MAP are well fitted by a single linear regression (Pearson correlation coefficient $R^2 = 0.79$, p-value $= 1.8 \times 10^{-7}$):

$$\delta^{15}N = -0.01 \times \left(PMAP\right) + 14.59 \quad (4)$$

This relation is likely valid because both ratites are mostly herbivorous feeders, inhabit semi-arid to arid climates, and occupy similar niches in their respective food webs. Accordingly, we can estimate PMAP at Lukenya Hill and Kisese II using this inverse relationship (Fig. 7).

Pristine δ^{15}N values of OES from Lukenya Hill range from 4.5‰ to 11.1‰, which correspond to PMAP values of ~900 to 310 mm/year, respectively, using Equation (4) (after Fig. 7). Mean δ^{15}N values become progressively less positive through time, corresponding with a progressive increase in PMAP over time. The lowest mean PMAP (386 ± 85 mm/yr) occurs 37.6–31.2 ka, and the highest mean PMAP (790 ± 103 mm/yr) occurs from 6.9 to 3.8 ka, higher than modern MAP at Lukenya Hill (~630 mm/year; McSweeney et al., 2012b).

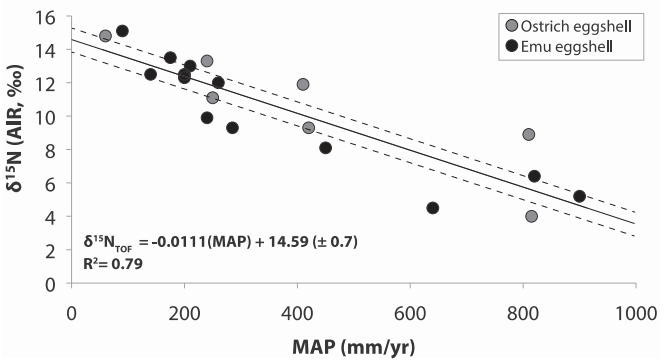

Fig. 7. Mean annual precipitation (MAP) versus δ^{15}N values of modern ostrich eggshell from South Africa (from Johnson et al., 1998) and emu eggshell from Australia (Newsome et al., 2011). Solid line is least squares best fit and dashed lines are 66.7% confidence interval.

δ^{15}N values from Kisese II range from 3.4 to 9.2‰, corresponding to PMAP from ~1010 to 490 mm/yr, respectively. In contrast to the progressive increase in PMAP at Lukenya Hill, δ^{15}N values of OES from Kisese II indicate mean rainfall throughout the record was subtly oscillating between drier and wetter periods. The wetter periods occur just before and after the temporal hiatus (mean PMAP = 727 ± 46 mm/yr from 39.6 to 34.4 ka, $n = 22$; 765 ± 32 mm/yr from 23.7 to 21.2 ka, $n = 9$), both which appear drier than present

conditions near Kisese II (McSweeney et al., 2012a). The drier periods are at the beginning of the record (mean PMAP = 646 ± 110 mm/yr from 46.8 to 41.7 ka, $n = 9$) and in the most recent interval in the Holocene (mean PMAP = 674 ± 54 mm/yr from 4.4. − 4.1 ka, $n = 5$). Dry intervals at Kisese II are significantly wetter than the drier intervals at Lukenya Hill.

4.3. Oxygen isotopes

The oxygen isotopic composition of OES calcite varies due to 1) temperature at formation, 2) kinetic and equilibrium effects during biomineralization, and 3) the $\delta^{18}O$ value of body water (hereafter, $\delta^{18}O_{bodyH2O}$). $\delta^{18}O_{bodyH2O}$ values depend on 4) atmospheric oxygen incorporated during respiration and digestion, 5) consumed waters, and 6) water lost via excretion or evaporation during respiration and thermoregulation (Koch, 1998; Luz et al., 1984). Ostriches are warm-blooded animals with stable body temperatures at ~39 °C (Crawford and Schmidt-Nielsen, 1967; Eagle et al., 2015), and since eggshells mineralize very rapidly, temperature and equilibrium effects can be considered constant during biomineralization and should not be reflected in changes in OES $\delta^{18}O$ values. Atmospheric oxygen $\delta^{18}O$ is roughly constant (~+24‰, VSMOW; Luz and Barkan, 2011) and atmospheric enrichment in ^{18}O (known as the Dole Effect) will result in more positive values of OES calcite $\delta^{18}O$ values. However, respiration and thermoregulation are non-constant and vary greatly with ambient temperature (Schmidt-Nielsen et al., 1969) given that ostriches do not have sweat glands and require increased respiration to thermoregulate. Unless the $\delta^{18}O$ value of atmospheric O_2 changed significantly in the past, we would expect the majority of changes in the $\delta^{18}O$ value of body water to derive from changes in $\delta^{18}O$ of consumed water. Like other animals deemed "evaporation-sensitive" (e.g., Levin et al., 2006), as non-obligate drinkers, ostriches derive most of their water from plant-leaf water. Therefore, we propose that $\delta^{18}O$ values in OES calcite should primarily reflect the oxygen isotopic composition of leaves, or foliar $\delta^{18}O$ (hereafter $\delta^{18}O_{foliarH2O}$).

4.3.1. Towards a measure of past evapotranspiration

$\delta^{18}O$ values of plant leaf water are controlled by the isotopic composition of meteoric water, which is modified by soil evaporation and transpiration. These processes are predominantly controlled by vapor pressure difference (i.e. relative humidity) and temperature (Barbour et al., 2004; Kahmen et al., 2011; Roden and Ehleringer, 1999). This results in higher $\delta^{18}O$ values of plant leaf water and derived cellulose than their sources. Since foliar $\delta^{18}O$ values will vary depending on photosynthetic pathway and ambient climatic variables (Epstein et al., 1977; Sternberg et al., 1984), variations of foliar $\delta^{18}O$ values through time should reflect relative changes in net evapotranspiration, whether driven by temperature, humidity, and/or physiological responses in the plant (if derived from a consistent meteoric water source; e.g., Dawson et al., 2002).

The fractionation factor (α) between ostrich body water and eggshell calcite ($\alpha_{calcite\text{-}bodyH2O} = 1.0379 \pm 0.002$; Passey et al., 2014) can be used to back-calculate the $\delta^{18}O_{bodyH2O}$ values. We can then quantify relative components contributing to body water using mass balance and determine $\delta^{18}O_{foliarH2O}$ values. A model by Kohn (1996) relates $\delta^{18}O$ values of biomineral apatite in obligate-drinking herbivorous birds and other fauna to $\delta^{18}O_{bodyH2O}$ values. This provides weighted estimates of each of the variables contributing to $\delta^{18}O_{bodyH2O}$ values. Modifying this model for non-obligate drinkers like ostriches, the largest source of oxygen to the diet is from foliar water (57%), with other contributions from atmospheric oxygen via respiration and thermoregulation (~30%), leaf cellulose oxygen (~9%), and oxygen from water vapor in air (4%, all after Kohn, 1996). These can be simplified to a linear relationship between body water and source water, namely, foliar water:

$$\delta^{18}O_{bodyH2O} = A + B * \delta^{18}O_{foliarH2O} \quad (5)$$

For herbivorous birds, A and B are 5.83‰ and 0.71, respectively (Kohn, 1996). Calculated $\delta^{18}O_{foliarH2O}$ values for each ancient OES $\delta^{18}O$ value in our study were determined by calculating $\delta^{18}O_{bodyH2O}$ and then solving Equation (5) for $\delta^{18}O_{foliarH2O}$ (supplementary data). Resultant $\delta^{18}O_{foliarH2O}$ values from these calculations will be referred to as derived from "model 1".

We can model the $\delta^{18}O_{foliarH2O}$ values another way, by using a model for the mean oxygen isotopic compositions of cellulose and leaf water in C_3 and C_4 plants in tropical semi-arid to arid climates (Sternberg et al., 1984). Sternberg et al. (1984) showed that measured $\delta^{18}O$ values of cellulose from C_3 and C_4 plants in hot semi-arid climates have a ~10‰ difference between C_3 and C_4 plant cellulose $\delta^{18}O$ values. This relationship can be used to estimate cellulose $\delta^{18}O$ values in tropical arid climates if the fraction of C_3 versus C_4 plants is known. Using our calculated dietary $\delta^{13}C$ values from measured OES $\delta^{13}C$ values, we can determine the fraction f of C_3 versus C_4 (i.e. non-C_3) plants in the diet using mass balance using the same linear two endmember mixing model (Section 2.1.1). For example, the fraction of C_4 plants in the diet can be determined as such:

$$f_{C4} = \left(\delta^{13}C_{diet} - \delta^{13}C_{C3}\right) \div \left(\delta^{13}C_{C4} - \delta^{13}C_{C3}\right) \quad (6)$$

Using average cellulose $\delta^{18}O$ values in C_3 and C_4 plants (Sternberg et al., 1984), we can calculate the $\delta^{18}O$ of cellulose derived from the ostrich diet directly:

$$\delta^{18}O_{cellulose} = \left(1 - f_{C4}\right) \times \delta^{18}O_{C3} + f_{C4} \times \delta^{18}O_{C4} \quad (7)$$

Then, we can calculate a $\delta^{18}O_{foliarH2O}$ value by using the relationship between oxygen isotopic compositions of leaf water and cellulose (e.g., Sternberg, 1989):

$$\delta^{18}O_{foliarH2O} \sim \delta^{18}O_{cellulose} - 27‰ \quad (8)$$

These derived $\delta^{18}O_{foliarH2O}$ values hereafter will be referred to as derived from "model 2" (Supplementary Data). In both models, lower $\delta^{18}O$ values should correspond with lower $\delta^{18}O_{foliarH2O}$ values and therefore decreased evapotranspiration, and higher $\delta^{18}O$ values correspond with higher modeled $\delta^{18}O_{foliarH2O}$ values and increased evapotranspiration.

4.3.2. $\delta^{18}O$ values as an evapotranspiration proxy at each locality

The ranges of OES $\delta^{18}O$ values are similar at the two localities. Individual OES $\delta^{18}O$ values at Lukenya Hill vary between 29.1 and 40.0‰ (Table 2). There are subtle shifts in mean values through time (Table 4 and Fig. 5), but they mostly fall within uncertainty of the preceding and following intervals. One exception occurs from 18.8 to 14.9 ka, when the mean $\delta^{18}O$ value (38.3 ± 1.1‰, $n = 7$) corresponds with higher evapotranspiration than the preceding interval outside of uncertainty (36.4 ± 0.2‰, $n = 4$, from ~26.3–21.6 ka).

At Kisese II, $\delta^{18}O$ values range from 28.8 to 39.7‰. Shifts in mean $\delta^{18}O$ values through time are again subtle and often within uncertainty of bounding intervals (Table 3 and Fig. 6). Minimum mean $\delta^{18}O$ values occur early in the record from ~46.9–41.7 ka (32.6 ± 2.4‰) and from ~18.1–4.2 ka (30.6 ± 2.0‰), corresponding with resolvable minima in mean evapotranspiration. Maximum mean $\delta^{18}O$ values = 35.6 ± 1.4‰ from (~23.7–21.2 ka), just after the hiatus in data, and they correspond with increased

evapotranspiration.

5. Discussion

The isotopic variation in OES allows us to assess the relationships between the three proxies and compare them to other environmental proxy records. OES isotope proxy records are discussed 1) relative to each element, including the utility of the foliar $\delta^{18}O$ models; 2) between localities, contextualized by co-occurring faunal and material culture records, including the MSA/LSA transition; 3) in the context of well-known paleoclimate events recorded in other records; and 4) compared to regional paleoclimate records. We then evaluate which potential dynamic processes may be recorded by the OES isotope proxy records.

5.1. Relations among isotope proxies

5.1.1. Correlations between the three isotope systems

Fig. 8 shows two-dimensional plots to assess correlations between isotope systems. If each isotope system is interpreted as an independent paleoenvironmental proxy, they should not vary systematically with respect to each other. If proxies are interrelated, we may observe correlations between some isotope systems. Statistical assessments are presented in Tables 6 and 7 as symmetric matrices. Pearson product-moment correlation coefficients (R) indicate small linear correlations between each isotope system (Table 6) and a non-parametric rank correlation test, Kendall's tau correlation coefficient (τ), also indicates weak correlation between the three systems (Table 7). The weakest correlations are between $\delta^{15}N$ and $\delta^{18}O$ values ($R^2 = 0.016$, $p > 0.05$; $\tau = 0.074$, $p > 0.05$), with p-values indicating that there is no statistically significant correlation between the two systems. The strongest correlations are between $\delta^{13}C$ and $\delta^{18}O$ values ($R^2 = 0.149$, $p < 0.05$; $\tau = 0.265$, $p < 0.05$). Correlations between $\delta^{15}N$ and $\delta^{13}C$ values are weak ($R^2 = 0.071$, $p < 0.05$; $\tau = 0.221$, $p < 0.05$), but both correlation pairs are statistically significant.

While there are no strong correlations between any two isotope variables, we can speculate how each proxy record may affect the others considering biological, climatological, and physiological processes. For example, $\delta^{15}N$ values may weakly co-vary with $\delta^{13}C$ values if plants adapted to drier climates, such as C_4 plants, increase in the diet during intervals with low PMAP. We may expect $\delta^{15}N$ values to co-vary with $\delta^{18}O$ values if precipitation is coupled with relative humidity. From these data, samples with estimated PMAP <500 mm/yr also all have $\delta^{18}O$ values > 34‰ (Fig. 8C), implying there may be a relationship between lower PMAP and higher $\delta^{18}O$ values. This may be due to coupling of low precipitation and decreased relative humidity. Subtle correlation between $\delta^{13}C$ and $\delta^{18}O$ values may be related to the photosynthetic pathway of the plants in the diet. More negative $\delta^{13}C_{diet}$ values in the data set (~−27 to −24‰) have lower $\delta^{18}O$ values ~ 28–35‰, and less negative $\delta^{13}C_{diet}$ values (~−22 to −15‰) have elevated $\delta^{18}O$ values (~33–40‰). These ranges in $\delta^{13}C_{diet}$ broadly correspond with C_3 versus C_4 plant types. An intermediate range of $\delta^{13}C_{diet}$ values (~−25 to −22‰), implying mixed C_3 - C_4 diets, corresponds with a broad range of $\delta^{18}O$ values (~29–39‰). Other studies have determined that faunal tooth enamel $\delta^{18}O$ values are affected by the paleodiet of the animal (Faith, 2018). We may expect increased $\delta^{18}O$ values to co-vary with higher dietary $\delta^{13}C$ values because C_4 plants are better adapted to environments with high temperatures, low humidity and low pCO_2 (Ehleringer et al., 1997). Higher OES $\delta^{18}O$ values may also be attributed to the physiological response of C_3 plants to increased temperatures and decreased humidity, when C_3 plants may shut down photosynthesis, resulting in enrichment in ^{18}O (e.g., Sternberg et al., 1984). Hence, it is not surprising that there is more variation in $\delta^{18}O$ values if there are mixed C_3 - C_4 diets.

Previous work interpreted OES $\delta^{18}O$ values as a qualitative

Table 7
Kendall's correlation coefficients τ and p-value in parentheses. Values are presented as a symmetric matrix. Null hypothesis is that there is no correlation between the variables in the row versus the column.

Kendall's τ (p-value)	$\delta^{13}C$	$\delta^{15}N$	$\delta^{18}O$
$\delta^{13}C$	1	0.221 (0.00129)	0.265 (6.229e-05)
$\delta^{15}N$	0.221 (0.00129)	1	0.074 (0.2803)
$\delta^{18}O$	0.265 (6.229e-05)	0.074 (0.2803)	1

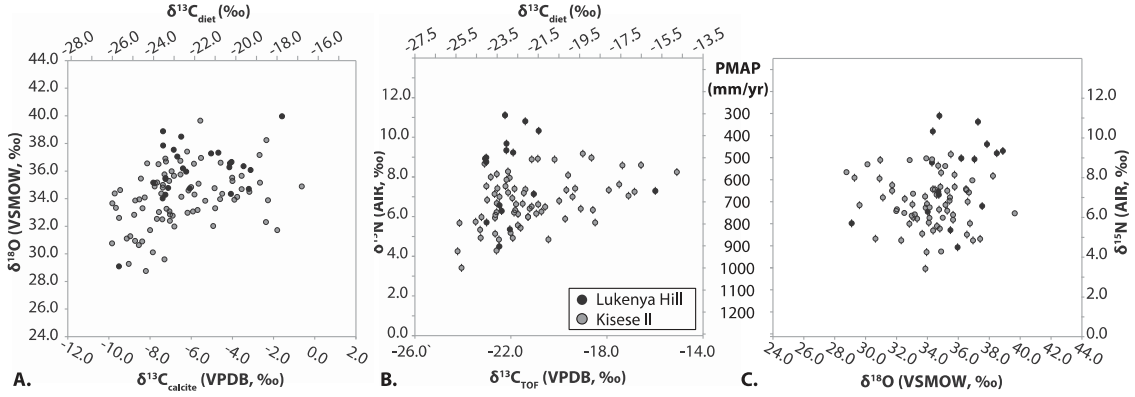

Fig. 8. Comparisons of each isotope system from OES results. There is a subtle positive correlation between $\delta^{18}O$ and $\delta^{13}C$ values (Pearson $R^2 = 0.15$).

Table 6
Pearson's correlation coefficient R, R^2 in brackets, and p-value in parentheses. Values are presented as a symmetric matrix. Null hypothesis is that there is no correlation between the variables in the row versus the column.

Pearson's R [R^2] (p-value)	$\delta^{13}C$	$\delta^{15}N$	$\delta^{18}O$
$\delta^{13}C$	1	0.267 [0.071] (0.00747)	0.386 [0.149] (4.861e-05)
$\delta^{15}N$	0.267 [0.071] (0.00747)	1	0.127 [0.016] (0.2105)
$\delta^{18}O$	0.386 [0.149] (4.861e-05)	0.127 [0.016] (0.2105)	1

aridity proxy (e.g., Lee-Thorp and Ecker, 2015; Roberts et al., 2016), in which case, we may expect a significant negative correlation between aridity and precipitation (and thus a positive correlation between $\delta^{18}O$ and $\delta^{15}N$ values). Here we have shown that $\delta^{18}O$ values do not have any statistically significant correlation with $\delta^{15}N$. Instead, OES $\delta^{18}O$ values appear to be responding to more than a single climatic/physiological variable. This may include precipitation amount, relative humidity, temperature, and plant transpiration (via plant photosynthetic pathway). Evapotranspiration incorporates these variables as an integrated signal from foliar $\delta^{18}O$ values. This is a more robust interpretation of OES $\delta^{18}O$ values, rather than interpreting it as an aridity proxy. In light of this, biomineral carbonate $\delta^{18}O$ values used as an aridity index in other paleo-studies should be interpreted with caution: without additional data to constrain other climatic variables, it will be challenging to robustly evaluate $\delta^{18}O$ values as a measure of aridity in isolation.

5.1.2. Assessing the foliar $\delta^{18}O$ models

A comparison of the two models (Fig. 9) shows there is a systematic offset towards higher calculated $\delta^{18}O_{foliarH2O}$ values from model 1 compared to model 2. The range of $\delta^{18}O_{foliarH2O}$ values for model 1 versus model 2 are [-0.4‰, 7.0‰] and [0.3‰, 4.9‰], respectively, while individual $\delta^{18}O_{foliarH2O}$ values differ between 0.1‰ and 4.6‰ (supplementary data). Model 1 may produce systematically elevated values with respect to model 2 because it explicitly considers other factors that may increase the $\delta^{18}O$ values of biominerals (such as respiration). Larger differences in the two model results may imply a greater contribution of other biological effects after foliar water consumption by ostriches that would result in enrichment in ^{18}O, such as increased respiration and/or thermoregulation.

With little primary foliar $\delta^{18}O$ data from eastern Africa to compare to the $\delta^{18}O_{foliarH2O}$ proxy values, we compare the results of each of our models to those produced by modeled modern foliar water $\delta^{18}O$ values in eastern Africa (West et al., 2008). The model by

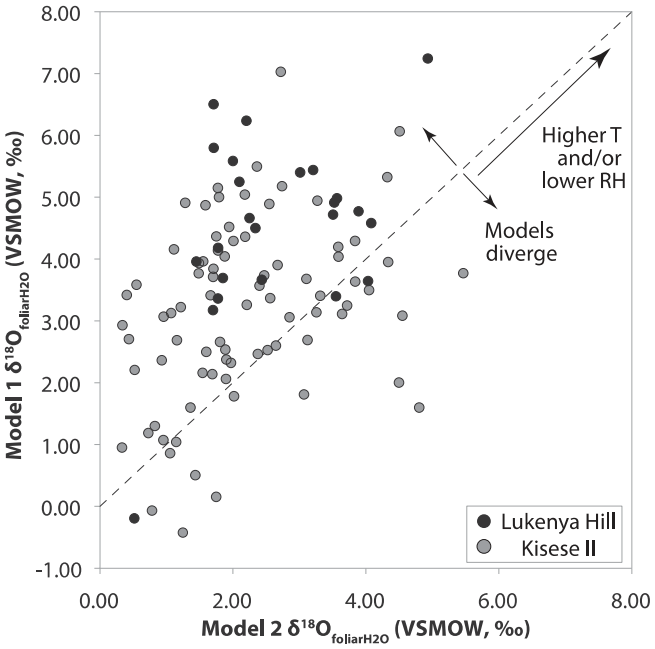

Fig. 9. Comparison of model $\delta^{18}O$ values. X-axis provides values calculated from model 2, and y-axis provides values are from model 1. Points near the 1:1 line (dashed) demonstrate good agreement between models; values in the more positive direction of either axis indicate higher temperatures (T) and/or lower relative humidity (RH).

West et al. (2008) is based on biophysical models of plant leaf isotope fractionation and local point precipitation isotope and climate data. Models 1 and 2, from the OES stable isotope data presented here, produce a similar range of values as the model by West et al. (2008) for equatorial and high-altitude Eastern African regions and tropical central/western African regions (range $\delta^{18}O_{foliarH2O}$ ~1–10‰; West et al., 2008: Fig. 1). Thus, our modeled $\delta^{18}O_{foliarH2O}$ values thus appear credible.

To provide a $\delta^{18}O_{foliarH2O}$ value as a proxy for evapotranspiration, Figs. 5 and 6 show OES $\delta^{18}O$ values on the upper x-axis, and calculated $\delta^{18}O_{foliarH2O}$ values on the lower x-axis using the approach of model 1. The $\delta^{18}O_{foliarH2O}$ values calculated from model 1 directly relate to the $\delta^{18}O$ values of OES calcite. This allows the discussion of $\delta^{18}O_{foliarH2O}$ values to remain independent with respect to the dietary $\delta^{13}C$ values, which contribute to the calculation of $\delta^{18}O_{foliarH2O}$ values in model 2. Further discussion of the two model results can be found in the Supplementary Materials.

5.2. Comparison between the OES isotope records at Lukenya Hill and Kisese II

We can compare the paleoenvironmental proxy data between sites through the ~50 ka interval, particularly with respect to archaeological change across the MSA/LSA transition at each site. The $\delta^{13}C_{diet}$ values from OES can also be compared to inferences made about local plant ecology as determined from corresponding faunal records.

At Lukenya Hill, individual $\delta^{13}C_{diet}$ values vary subtly through time, but mean values indicate a mixed to dominantly C_4 plant diet in most intervals. Faunal analyses at Lukenya Hill indicate a predominantly C_4-rich landscape throughout the ~50 ka interval, though several arid-adapted taxa (e.g., *Equus grevyi, Oryx beisa,* and *Damaliscus hypsodon*) disappear at the onset of the Holocene (Faith et al., 2012; Marean, 1992, 1991; Robinson, 2017). At Kisese II, mean values subtly oscillate between mixed and C_3-dominant diets: lowest mean $\delta^{13}C$ values, indicative of C_3-dominant diets, occur ~35.9–34.3 ka and 23.7–23.1 ka. Faunal analyses from Kisese II are challenging to interpret due to the incompleteness of the available collection (Tryon et al., 2019). Like Lukenya Hill, Kisese II appears to record the loss of *E. grevyi*, *O. beisa*, and *D. hypsodon* by the Holocene (Marean and Gifford-Gonzalez, 1991), but available fauna generally indicate diverse grassland and wooded ecosystems in contrast to the abundant grazers of Lukenya Hill (Tryon et al., 2019). This is generally in agreement with the OES dietary $\delta^{13}C$ values.

Unlike the carbon isotopes, mean values in nitrogen isotopic compositions at the two sites show distinct PMAP amounts and trends through time (Figs. 5 and 6). Precipitation gradually increases through time at Lukenya Hill from an arid to semi-arid climate, while at Kisese II, precipitation patterns oscillate between wet and dry within the range of semi-arid to temperate climates. The $\delta^{15}N$ values indicate that, as is the case today, Kisese II had generally higher precipitation than Lukenya Hill in the past. However, the nature of temporal variation differs at each site. There is modest oscillatory variation in mean PMAP at Kisese II, while PMAP at Lukenya Hill steadily increases through time to a maximum in the later Holocene that is wetter than it is today. These results may be readily reconciled with the faunal record at Lukenya Hill and confirm that the observed local extirpation of arid-adapted fauna was driven by increases in precipitation rather than changing local vegetation (cf. Marean, 1992; Faith, 2014). The two records also share some common characteristics. For example, relative minima in mean PMAP occur at the earliest intervals, and similar maximum values of PMAP are observed at the two sites, greater than ~900 mm/yr (OES with $\delta^{15}N$ values < 4.6‰).

At Lukenya Hill, highest mean $\delta^{18}O_{foliarH2O}$ values occur in both

models between ~26.3–21.6 ka and 18.8–14.9 ka, implying increased evapotranspiration during intervals of intermediate PMAP and a C_4-rich ostrich diet (Fig. 5). Because C_4 plants are better adapted to arid environments and are relatively abundant there, high $\delta^{18}O_{foliarH2O}$ values at Lukenya Hill may be responding to changes in temperature and/or physiological adaptation of C_4 plants to arid climates.

At Kisese II, mean $\delta^{18}O_{foliarH2O}$ values are higher in intervals with higher PMAP and more C_3 plants in the diet, indicating wetter, more C_3-rich intervals are characterized by higher evapotranspiration (Fig. 6). The trend of higher PMAP and concomitant evapotranspiration may imply a temperature control on $\delta^{18}O_{foliarH2O}$ values here (if precipitation and relative humidity are coupled). This relationship is apparent from ~35.1–33.7 ka and ~23.7–21.2 ka. If precipitation and relative humidity are coupled, intervals with lower $\delta^{18}O_{foliarH2O}$ values may similarly reflect lower temperatures, such as from ~46.9–41.7 ka and from ~17.6 ka into the Holocene (Fig. 6).

The OES stable isotope proxies indicate subtle but distinct trends in the paleoenvironments of Kisese II and Lukenya Hill through time, including across the MSA/LSA transitions (Figs. 5 and 6). Of the three isotope proxy records, PMAP at the two sites contrasts most during their respective MSA/LSA transitions. At Kisese II, a maximum in PMAP and high evapotranspiration occurs during the onset of the MSA/LSA transition, when the ostrich diets were dominated by C_3 plants. During the MSA/LSA transition at Lukenya Hill, PMAP was lowest, C_4 plants were relatively abundant, and there was relatively moderate temperature and/or aridity. Dietary $\delta^{13}C$ values indicate vegetation was consistently more C_4-rich at Lukenya Hill than at Kisese II. These differences provide little direct support for a role for distinct environmental shifts as a key driver for the behavioral changes expressed as the MSA/LSA transition.

5.3. Localized expression of regional paleoclimate events

The OES isotope records provide the novel capability of examining how global or hemispheric climate events such as the Last Glacial Maximum and African Humid Period were expressed at the study sites, as described below.

5.3.1. Lukenya Hill and Kisese II during the Last Glacial Maximum (~26–19 ka)

There were drier and cooler climates in eastern Africa during the Last Glacial Maximum (LGM, ~26–19 ka; Clark et al., 2009), an interval defined by large Northern Hemisphere ice sheets and lower pCO_2 (Johnson, 2017; Petit et al., 1999). Such conditions would favor higher proportions of C_4 plants, lower PMAP, and/or increased evapotranspiration (if humidity is coupled with precipitation).

There is no significant change in $\delta^{13}C_{diet}$ values at Lukenya Hill during the LGM, but PMAP and $\delta^{18}O_{foliarH2O}$ values are gradually increasing. Increasing PMAP is in contrast with the notion that there were relatively drier climates in eastern Africa during the LGM, and paired with higher $\delta^{18}O_{foliarH2O}$ values, the local paleoenvironment at Lukenya Hill may be out of phase with larger scale climate trends in this interval.

At Kisese II, one of two maxima in PMAP occur at the beginning of the LGM. Eleven out of 26 OES reflect some dietary contribution from C_4 plants during the LGM, with relative increases in C_4 contribution (increased $\delta^{13}C_{diet}$ values) through the LGM (Fig. 6). This subtle shift in diet may reflect an increase in vegetation adapted to increased aridity and/or temperature. It could reflect an ecological response to lower pCO_2 during the LGM interval (Petit et al., 1999): because C_4 plants function better than C_3 plants in low pCO_2 regimes, they may expand their abundance and/or range in such climates (e.g., Ehleringer et al., 1997). Likewise, C_3 plants may become enriched in heavy isotopes in water-starved environments (Sternberg et al., 1984). High $\delta^{18}O_{foliarH2O}$ values, combined with a relative increase in C_4 plants in this interval, may indicate an adaptive ecological response of increased C_4 vegetation to lower pCO_2 during the LGM.

5.3.2. Lukenya Hill and Kisese II during the African Humid Period (~14–5 ka)

The African Humid Period (AHP, ~14–5 ka; DeMenocal et al., 2000; Shanahan et al., 2015) is defined by a period of higher rainfall across circum-Saharan Africa while the Sahara itself supported grass, trees, and lacustrine ecosystems. At Lukenya Hill, while $\delta^{13}C_{diet}$ and $\delta^{18}O$ values reflect no major changes relative to previous intervals, peak mean PMAP values at Lukenya Hill in the Holocene are greater than those of all previous intervals and modern MAP (~630 mm/year). This is consistent both with increased precipitation during the African Humid Period compared to prior intervals and with a drier Late Holocene, supporting other evidence that the AHP interval was wetter than it is today (Shanahan et al., 2015). This is also the largest shift in isotope values of any proxy record from either site, and it occurs in an interval known to host wetter climates evidenced in many diverse local to global-scale proxy records (e.g., Adkins et al., 2006; Cuffey et al., 2016; DeMenocal et al., 2000; McGee et al., 2013; McGee and deMenocal, 2017; Schefuβ et al., 2005; Shanahan et al., 2015). This lends further confidence to the fidelity of the $\delta^{15}N$ proxy for paleo-precipitation. PMAP at Kisese II does not increase to its maximum mean value during the African Humid Period, but the ages of the available OES are poorly constrained and the data are sparse in this interval.

5.4. Comparing OES proxies with regional paleoclimate records

With the three isotope systems in OES from Kisese II and Lukenya Hill, we can clarify how local environmental changes compare with regional records. There appear to be some agreements between records and, in other cases, contradictions. The $\delta^{15}N$-PMAP proxy allows assessment of wet and dry intervals compared to nearby lacustrine records, summarized in Fig. 10. The

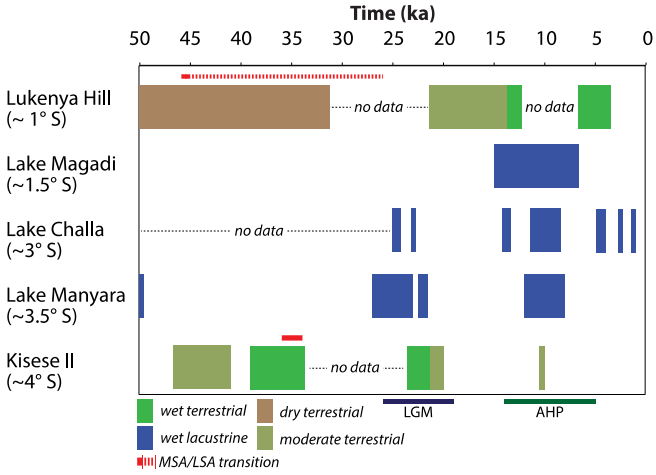

Fig. 10. Summary of wet intervals over the last ~50 ka from the sites discussed as compared to proximal lakes. Qualitative, relative indicators of wet intervals are indicated from proxies from lake records near Kisese II and Lukenya Hill compared to relative wet and dry intervals at the sites indicated from the $\delta^{15}N$ PMAP proxy. Unmarked intervals in lacustrine records lack evidence of wet climates. The MSA/LSA transition at each locality is also highlighted (red bars) along with the Last Glacial Maximum (LGM) and the African Humid Period (AHP). The proxy records come from the following published literature: Lake Magadi (Owen et al., 2019, 2018); Lake Challa (Verschuren et al., 2009); Lake Manyara (Bachofer et al., 2018; Casanova and Hillaire-Marcel, 1992).

OES stable isotope records at Kisese II and Lukenya Hill clearly record one or more of the "humid" intervals evidenced in proximal lacustrine records, but the archaeological and proximal lacustrine records do not agree in all intervals. For example, all of the nearby lacustrine records display evidence of a wetter AHP, as does the record at Lukenya Hill. Lake Magadi and Lake Manyara show contrasting responses to the LGM (Casanova and Hillaire-Marcel, 1992; Owen et al., 2019, 2018). Furthermore, the Lake Magadi record demonstrates progressive aridification following the LGM until the AHP, indicated by increases in local, woodland, and afromontane pollen (Owen et al., 2019). This is unlike the nearby Lukenya Hill OES isotope record which becomes progressively wetter through time up to the AHP. Nearby Kisese II, Lake Manyara records lake level transgressions just before and through the LGM, and again at the onset of the Holocene, identifying these as "humid" periods (Bachofer et al., 2018; Casanova and Hillaire-Marcel, 1992). The OES isotope record at Kisese II agrees with part of the Lake Manyara record, particularly regarding the wetter LGM. However, Lake Manyara shows no evidence of a wetter interval from ~39 to 34 ka, as is indicated by the PMAP and vegetation proxies at Kisese II. The Lake Challa record has the most in common with the Kisese II PMAP record, indicative of a wet LGM and a drier mid-Holocene (during the AHP), which is attributed to changes in the intensity of the African monsoon (Tierney et al., 2011b; Verschuren et al., 2009). Lake Eyasi, while proximal to Kisese II, hosts nearby archaeology and fossils which have been recently dated to ~115 ka, contesting previous ages of ~35 ka (Domínguez-Rodrigo et al., 2007; Domínguez-Rodrigo et al., 2008). This record is difficult to reconcile chronologically with our data and thus has not been included in our comparisons.

Farther afield, other records similarly corroborate the expression of localized environmental differences. At Lake Malawi (farther south of Kisese II), proxies indicate variation between wooded grasslands and woodlands over the last ~50 ka with progressive increases in wetness and temperatures, particularly by the LGM (Johnson et al., 2016). This again agrees with a wetter LGM, but it differs with respect to precipitation trends through time relative to the Kisese II PMAP proxy record. Also south of Kisese II, the Congo Fan record (~5.5° S latitude; Schefuβ et al., 2005) indicates that the AHP terminated later with decreasing latitudes into the Southern Hemisphere, in agreement with Shanahan et al. (2015). While the AHP is apparent at Lukenya Hill, the Congo Fan record is closer in latitude to Kisese II (4.42° S), which does not reflect a relatively wet interval during the AHP.

OES stable isotope data suggest that Lukenya Hill (~1° S) and Kisese II (~4° S) straddle an important boundary in Late Pleistocene climate systems that serve to emphasize the importance of local-scale reconstructions for comparison with hominid[1] behavioral change preserved in the archaeological record. Blome et al. (2012) divide eastern Africa from tropical Africa at about ~1° S latitude, and differences in the local paleoenvironmental records at Lukenya Hill and Kisese II corroborate diverse climate regimes across this ~1° S boundary. They also imply that general trends in a regionally wetting or drying climate apparent in lacustrine records do not necessarily apply at the habitat scale precisely.

5.5. Possible drivers of diverse local paleoenvironments

Contrasting relationships between the three isotopes at each locality imply that precipitation, humidity, temperature, and vegetation may not co-vary analogously in each place. Differences in humidity, temperature, and/or precipitation could be controlled by the same dynamic variables at the two localities, but their relative geographic positions may result in absolute differences in the coupling of these climate variables. For example, PMAP trends at Lukenya Hill may follow trends associated with the African monsoon (e.g., Shanahan et al., 2015), as indicated by the presence of an AHP maximum in rainfall. PMAP at Kisese II was subtly oscillatory and may be associated with glacial and interglacial cycles, but additional temporally highly resolved data, particularly in the hiatus, would be needed to assess this carefully. Tierney et al. (2011a) propose that contributing rainfall from different sources, such as the Atlantic and Indian Oceans, may contribute to the increase in net rainfall during the AHP. Since a wetter AHP is only seen at one of the two localities studied here (Lukenya Hill), PMAP there may partly reflect different geographic sources of precipitation between low southern hemisphere and equatorial latitudes. If this is the case, this would in turn affect the bulk meteoric water $\delta^{18}O$ values if multiple water sources contribute to foliar water $\delta^{18}O$ at one site but not at another site. However, changes in sea surface temperatures over the Indian Ocean can also affect rainfall amount over the two localities (e.g., Shanahan et al., 2015). Eastern African equatorial meteoric waters derive mainly from the Indian ocean via the Somali (and more locally, the Turkana) Jet(s), whose trajectories are strongly influenced by the steep altitudinal gradients characterizing the eastern African highlands (Nicholson, 2017, and references therein). Differences in atmospheric pressure controlled by the strength of the Turkana Jet may lead to variation in wind patterns and precipitation over these two localities and possibly differences in humidity and/or air temperatures not related to different precipitation sources. Hence, it is not necessary to invoke multiple sources of precipitation to produce different rainfall intensities over small distances.

Alternatively, different or shifting dynamic mechanisms may be responsible for diverse climates at each locality. For example, the Intertropical Convergence Zone (ITCZ)[2] might undergo secular latitudinal shifts through time (e.g., Blome et al., 2012) and control un-correlated precipitation changes at both sites. The Lake Challa record indicates that at equatorial latitudes, the ITCZ may experience shifts in mean annual position over orbital timescales which can lead to compression of the tropical convective zone (Verschuren et al., 2009). This may lead to different dynamic processes governing rainfall over a range of near-equatorial latitudes, such as the ITCZ, and its position relative to the Turkana Low Level Jet (e.g., Hartman, 2018; Nicholson, 2016, 2017). This may explain the distinct relationships between precipitation and climatic variables controlling evapotranspiration (humidity and/or temperature) differences in rainfall amount, and differing rainfall and vegetation trends through time.

5.6. Summary

Blome et al. (2012) speculated that hominid "populations in equatorial and eastern Africa may have been buffered from the extremes of climate change by locally steep altitudinal and rainfall gradients" (Blome et al., 2012: 563). However, data to reconstruct the mosaic of paleoenvironments available to hominids through time do not yet exist. For example, if the variability of environments were correlated with human innovation, such as the transition to the Later Stone Age technologies, we would expect the paleoenvironments to differ during the MSA/LSA transition relative to

[1] For clarity, the term "hominid" is defined here to include all taxa on the human lineage after the last common ancestor between chimpanzees and humans.

[2] The ITCZ is a belt of low pressure which circles the Earth generally near the equator where the trade winds of the Northern and Southern Hemispheres come together.

preceding intervals. However, consistent though subtle environmental change for the past ~50 ka appears to be the norm rather than the exception at both localities. At any point in the last ~50 ka, Lukenya Hill and Kisese II were environmentally distinct, and transitioned to subtly different environments over ~ multi-ka timescales (the temporal resolution at which we can assess most climate and archaeological records of interest). For example, the Lukenya Hill OES isotopic record shows evidence of a dry, C_4-rich, moderately arid and/or warm environment throughout the MSA/LSA transition. In contrast, the wettest intervals at Kisese II coincide with the LGM and the 36–34 ka interval coincident with the onset of the MSA/LSA transition there. If the environments at these two localities were always different from one another and were also subtly changing through time, the time-transgressive MSA/LSA transitions occurring in different paleoclimates across a distance <350 km cannot be explained as an adaptive response to absolute differences or similarities in environments, a specific environmental change, or to the tempo of such of changes. This implies that the origin(s) and spread of LSA technologies is in response to other, non-environmental causes.

6. Conclusions

The diverse and unique paleoenvironments through space and time at Kisese II and Lukenya Hill highlight the need for localized, precisely and accurately dated paleoenvironmental records in order to assess possible correlations between human evolution, innovation, and environmental change (e.g., Robinson, 2017). Analyses of ostrich eggshell fragments from the Lukenya Hill and Kisese II sequences, brought to these sites by humans, allow reconstruction of past local environments directly relevant to human subsistence. Modern calibrations of ostrich eggshells provide a basis to interpret the isotopic compositions of carbon in OES as a proxy for paleo-diet (Johnson et al., 1998). Modern nitrogen isotope data for ostrich and emu eggshells (Johnson et al., 1998; Newsome et al., 2011), first combined here, provide a proxy for mean annual precipitation. We propose a model to interpret the oxygen isotopic composition of OES as a novel proxy for evapotranspiration. Trends indicated by $\delta^{13}C$, $\delta^{15}N$ and $\delta^{18}O$ values of ostrich eggshell complement other proxy records that highlight large-scale changes in climate, such as the identification of the African Humid Period at Lukenya Hill, the Last Glacial Maximum at Kisese II, and time-transgressive variations in precipitation with latitude. However, the isotopic composition of OES may reveal changes in local climate more relevant to human subsistence in a given locality than those typically determined from regional scale proxy records. This is exemplified here by the differences in the OES isotope proxies compared to proximal lacustrine records, and in the coupling of temperature and/or relative humidity (inferred from $\delta^{18}O$ values) compared to the changes in rainfall or vegetation (derived from $\delta^{15}N$ or $\delta^{13}C$ values, respectively) at the two localities. Different dynamic processes may be responsible for the diverse paleoenvironments across equatorial latitudes, or site position relative to a process that undergoes secular shifts, such as the position of the ITCZ relative to the Turkana Jet. Other frequently used paleoclimate proxy records, such as ocean or lake cores, may not capture such mesoscopic variability in climate as is possible with the isotope systems of OES.

The integrated three-isotope approach applied at two eastern African archaeological localities demonstrates variable localized paleoenvironments from ~50 ka onward where environmental change (changing precipitation, vegetation, and temperature and/or relative humidity) is the norm rather than the exception. These records show that there is no significant environmental change leading into or during the MSA/LSA transitions at the sites. Populating the landscape with highly resolved local OES isotope records from archaeological sites could allow more direct assessment of the relationship between environmental and archaeological change at a highly resolved spatial scale. The results from Kisese II and Lukenya Hill also mark the first published use of stable isotopes in the organic fraction of ostrich eggshells at eastern African archaeological sites. These data derive from significantly older eggshells than previously studied African archaeological OES assemblages, demonstrating the potential to apply these methods to other African sites well into the Late Pleistocene. With the abundance of OES at archaeological sites across the African continent and beyond, and recent development of $^{230}Th/U$ burial dating of ostrich eggshell (Sharp et al., 2019), there is potential to build site-specific, precisely dated paleoenvironmental records up to ~10 times the ~50 ka limit of ^{14}C dating.

Declaration of competing interest

None.

Acknowledgements

This research is based on work supported by the National Science Foundation [grant number BCS-1727085] to W.D.S. and C.A.T., Harvard University, the American School of Prehistoric Research, a UC Berkeley Graduate Fellowship, and the Ann & Gordon Getty Foundation. Samples were acquired with permits to Tryon (including NCST/5/002/R/576 from the Government of the Republic of Kenya while an affiliate of the National Museums of Kenya, and No. 2014-231-NA-2013-122 and No. 2015-115-ER-2013-122 issued by the Tanzanian Commission for Science and Technology and to Lewis (Tanzanian COSTECH No. 201702-NA-2013-122). We thank the constructive and thoughtful reviews from two anonymous reviewers. We thank students from the UC Berkeley graduate discussion "IsoTopics" for feedback and constructive discussions, and Sydney Moss for assistance with photography and sample preparation.

Appendix A. Supplementary data

Supplementary data to this article can be found online at https://doi.org/10.1016/j.quascirev.2019.106142.

References

Adams, W.M., Goudie, A.S., Orme, A.R. (Eds.), 1996. The Physical Geography of Africa. Oxford University Press, Oxford.

Adkins, J., deMenocal, P., Eshel, G., 2006. The "African humid period" and the record of marine upwelling from excess 230Th in Ocean Drilling Program Hole 658C. Paleoceanography 21, 8305. https://doi.org/10.1029/2005PA001200.

Ambrose, S., DeNiro, M., 1986. The isotopic ecology fo east african mammals. Oecologia 69, 395–406. https://doi.org/10.1007/BF00377062.

Ambrose, S.H., 1998. Chronology of the later stone age and food production in East Africa. J. Archaeol. Sci. 25, 377–392. https://doi.org/10.1006/jasc.1997.0277.

Ambrose, S.H., 2001. Middle and later stone age settlement patterns in the central rift valley, Kenya: comparisons and contrasts. In: Conard, N.J. (Ed.), Settlement Dynamics of the Middle Paleolithic and Middle Stone Age. Kerns Verlag, Tiibingen, pp. 21–43. https://doi.org/10.1016/j.quaint.2017.03.027.

Amundson, R., Austin, A.T., Schuur, E.A.G., Yoo, K., Matzek, V., Kendall, C., Uebersax, A., Brenner, D., Baisden, W.T., 2003. Global patterns of the isotopic composition of soil and plant nitrogen. Glob. Biogeochem. Cycles 17. https://doi.org/10.1029/2002GB001903.

Austin, A.T., Sala, O.E., 1999. Foliar $\delta^{15}N$ is negatively correlated with rainfall along the IGBP transet in Australia. Aust. J. Plant Physiol. 26, 293–295. https://doi.org/10.1071/PP97167.

Bachofer, F., Queneherve, G., Hertler, C., Giemsch, L., Hochschild, V., Maerker, M., 2018. Paleoenvironmental research in the semiarid Lake Manyara area, northern Tanzania: a synopsis. In: Digital Geoarchaeology, pp. 123–138. https://doi.org/10.1007/978-3-319-25316-9.

Bahain, J.-J., Hovers, E., Leplongeon, A., Pearson, O., Fragnol, C., Douville, E., Hernandez, M., Tribolo, C., Pleurdeau, D., Puaud, S., Assefa, Z., Martin, L., Chapon, C., Asrat, A., 2017. Across the gap: geochronological and

sedimentological analyses from the late pleistocene-holocene sequence of goda buticha, southeastern Ethiopia. PLoS One. https://doi.org/10.1371/journal.pone.0169418.
Barbour, M.M., Roden, J.S., Farquhar, G.D., Ehleringer, J.R., 2004. Expressing leaf water and cellulose oxygen isotope ratios as enrichment above source water reveals evidence of a péclet effect. Oecologia 138, 426–435. https://doi.org/10.1007/s00442-003.
Bird, M.I., Turney, C.S.M., Fifield, L.K., Smith, M.A., Miller, G.H., Roberts, R.G., Magee, J.W., 2003. Radiocarbon dating of organic- and carbonate-carbon in Genyornis and Dromaius eggshell using stepped combustion and stepped acidification. Quat. Sci. Rev. 22, 1805–1812. https://doi.org/10.1016/S0277-3791(03)00151-3.
Blegen, N., 2017. The earliest long-distance obsidian transport: evidence from the ~200 ka middle stone age sibilo School road site, baringo, Kenya. J. Hum. Evol. 103, 1–19. https://doi.org/10.1016/j.jhevol.2016.11.002.
Blome, M.W., Cohen, A.S., Tryon, C.A., Brooks, A.S., Russell, J., 2012. The environmental context for the origins of modern human diversity: a synthesis of regional variability in African climate 150,000-30,000 years ago. J. Hum. Evol. 62, 563–592. https://doi.org/10.1016/j.jhevol.2012.01.011.
Bronk-Ramsey, C., 2001. OxCal [WWW Document].
Bronk Ramsey, C., 2016. Development of the radiocarbon calibration program. Radiocarbon 43, 355–363. https://doi.org/10.1017/s0033822200038212.
Brooks, A.S., Hare, P.E., Kokis, J.E., Miller, G.H., Ernst, R.D., Wendorf, F., 1990. Dating pleistocene archeological sites by protein diagenesis in ostrich eggshell. Science 248, 60–64. https://doi.org/10.1126/science.248.4951.60.
Brown, K.S., Marean, C.W., Jacobs, Z., Schoville, B.J., Oestmo, S., Fisher, E.C., Bernatchez, J., Karkanas, P., Matthews, T., 2012. An early and enduring advanced technology originating 71,000 years ago in South Africa. Nature 491, 590–593. https://doi.org/10.1038/nature11660.
Bwasiri, E.J., Smith, B.W., 2015. The rock art of Kondoa District, Tanzania. Azania 50, 437–459. https://doi.org/10.1080/0067270X.2015.1120436.
Casanova, J., Hillaire-Marcel, C., 1992. Chronology and paleohydrology of late quaternary high lake levels in the Manyara basin (Tanzania) from isotopic data (^{18}O, ^{13}C, ^{14}C, Th/U) on fossil stromatolites. Quat. Res. 38, 205–226.
Cerling, T.E., Harris, J.M., Passey, B.H., 2003. Diets of east african bovidae based on stable isotope analysis. J. Mammal. 84, 456–470. https://doi.org/10.1644/1545-1542(2003)084<0456:doeabb>2.0.co;2.
Cerling, T.E., Hay, R.L., 1986. Study of paleosol carbonates from olduvai gorge. Quat. Res. 25, 63–78.
Cerling, T.E., Wynn, J.G., Andanje, S.A., Bird, M.I., Korir, D.K., Levin, N.E., MacE, W., MacHaria, A.N., Quade, J., Remien, C.H., 2011. Woody cover and hominin environments in the past 6-million years. Nature 476, 51–56. https://doi.org/10.1038/nature10306.
Cheng, H., Edwards, R.L., Southon, J., Matsumoto, K., Feinberg, J.M., Sinha, A., Zhou, W., Li, H., Li, X., Xu, Y., Chen, S., Tan, M., Wang, Q., Wang, Y., Ning, Y., 2018. Atmospheric 14C/12C changes during the last glacial period from Hulu Cave. Science 362, 1293–1297. https://doi.org/10.1126/science.aau0747.
Clark, P.U., Dyke, A.S., Shakun, J.D., Carlson, A.E., Clark, J., Wohlfarth, B., Mitrovica, J.X., Hostetler, S.W., McCabe, A.M., 2009. The last glacial maximum. Science 325, 710–714. https://doi.org/10.1126/science.1172873.
Coplen, T.B., 1996. New guidelines for reporting stable hydrogen, carbon, and oxygen isotope-ratio data. Geochem. Cosmochim. Acta 60, 3359–3360.
Cornwell, W.K., Wright, I., Turner, J., Maire, V., Barbour, M., Cernusak, L., Dawson, T., Ellsworth, D., Farquhar, G., Griffiths, H., Keitel, C., Knohl, A., Reich, P., Williams, D., Bhaskar, R., Cornelissen, J.H.C., Richards, A., Schmidt, S., Valladares, F., Körner, C., Schulze, E.D., Buchmann, N., Santiago, L., 2016. A global dataset of leaf delta 13C values. Sci. Data.
Cornwell, W.K., Wright, I.J., Turner, J., Maire, V., Barbour, M.M., Cernusak, L.A., Dawson, T., Ellsworth, D., Farquhar, G.D., Griffiths, H., Keitel, C., Knohl, A., Reich, P.B., Williams, D.G., Bhaskar, R., Cornelissen, J.H.C., Richards, A., Schmidt, S., Valladares, F., Körner, C., Schulze, E.D., Buchmann, N., Santiago, L.S., 2018. Climate and soils together regulate photosynthetic carbon isotope discrimination within C3 plants worldwide. Glob. Ecol. Biogeogr. 27, 1056–1067. https://doi.org/10.1111/geb.12764.
Craine, J., Craine, J.M., Elmore, A.J., Aidar, M.P.M., Bustamante, M., Dawson, T.E., Hobbie, E.A., Kahmen, A., Mack, M.C., Mclauchlan, K.K., Michelsen, A., Nardoto, G.B., Pardo, L.H., 2009. Global patterns of foliar nitrogen isotopes and their relationships with climate. mycorrhizal fungi 980–992. https://doi.org/10.1111/j.1469-8137.2009.02917.x.
Crawford, E.C., Schmidt-Nielsen, K., 1967. Temperature regulation and evaporative cooling in the ostrich. Am. J. Physiol. 212, 347–353.
Cuffey, K.M., Clow, G.D., Steig, E.J., Buizert, C., Fudge, T.J., Koutnik, M., Waddington, E.D., Alley, R.B., Severinghaus, J.P., 2016. Deglacial temperature history of West Antarctica. Proc. Natl. Acad. Sci. U.S.A. 113, 14249–14254. https://doi.org/10.1073/pnas.1609132113.
Dawson, T.E., Mambelli, S., Plamboeck, A.H., Templer, P.H., Tu, K.P., 2002. Stable isotopes in plant ecology. Annu. Rev. Ecol. Systemat. 33, 507–559. https://doi.org/10.1146/annurev.ecolsys.33.020602.095451.
Demarchi, B., Hall, S., Roncal-Herrero, T., Freeman, C.L., Woolley, J., Crisp, M.K., Wilson, J., Fotakis, A., Fischer, R., Kessler, B.M., Jersie-Christensen, R.R., Olsen, J.V., Haile, J., Thomas, J., Marean, C.W., Parkington, J., Presslee, S., Lee-Thorp, J., Ditchfield, P., Hamilton, J.F., Ward, M.W., Wang, C.M., Shaw, M.D., Harrison, T., Domínguez-Rodrigo, M., Macphee, R.D.E., Kwekason, A., Ecker, M., Horwitz, L.K., Chazan, M., Kroger, R., Thomas-Oates, J., Harding, J.H., Cappellini, E., Penkman, K., Collins, M.J., 2016. Protein sequences bound to mineral surfaces persist into deep time. Elife 5. https://doi.org/10.7554/eLife.17092.
DeMenocal, P., Ortiz, J., Guilderson, T., Adkins, J., Sarnthein, M., Baker, L., Yarusinsky, M., 2000. Abrupt onset and termination of the African Humid Period: rapid climate responses to gradual insolation forcing. Quat. Sci. Rev. 19, 347–361. https://doi.org/10.1016/S0277-3791(99)00081-5.
DeNiro, M.J., Epstein, S., 1981. Influence of diet on the distribution of nitrogen isotopes in animals. Geochem. Cosmochim. Acta 45, 341–351. https://doi.org/10.1016/0016-7037(81)90244-1.
Domínguez-Rodrigo, M., Díez-Martín, F., Mabulla, A., Luque, L., Alcalá, L., Tarriño, A., López-Sáez, J.A., Barba, R., Bushozi, P., 2007. The archaeology of the middle pleistocene deposits of Lake Eyasi, Tanzania. J. Afr. Archaeol. 5, 47–75. https://doi.org/10.3213/1612-1651-10085.
Domínguez-Rodrigo, M., Mabulla, A., Luque, L., Thomson, J., Rink, J., Diez, F., Bushozi, P., Alcalá, L., 2008. A new archaic Homo sapiens fossil from Lake Eyasi. Journal of Human Evolution 54 (6), 899–903. https://doi.org/10.1016/j.jhevol.2008.02.002.
Eagle, R.A., Enriquez, M., Grellet-Tinner, G., Pérez-Huerta, A., Hu, D., Tütken, T., Montanari, S., Loyd, S.J., Ramirez, P., Tripati, A.K., Kohn, M.J., Cerling, T.E., Chiappe, L.M., Eiler, J.M., 2015. Isotopic ordering in eggshells reflects body temperatures and suggests differing thermophysiology in two Cretaceous dinosaurs. Nat. Commun. 6, 1–11. https://doi.org/10.1038/ncomms9296.
Ehleringer, J.R., Cerling, T.E., 2002. C_3 and C_4 photosynthesis. Encycl. Glob. Environ. Chang. 2, 186–190.
Ehleringer, J.R., Cerling, T.E., Helliker, B.R., 1997. C_4 photosynthesis, atmospheric CO_2, and climate. Oecologia 112, 285–299. https://doi.org/10.1007/s004420050311.
Epstein, S., Thompson, P., Yapp, C.J., 1977. Oxygen and hydrogen isotopic ratios in plant cellulose. Science 198, 1209–1215.
Faith, J., 2014. Late pleistocene and holocene mammal extinctions on continental Africa. Earth-Sci. Rev. 128, 105–121.
Faith, J.T., 2018. Paleodietary change and its implications for aridity indices derived from δ18O of herbivore tooth enamel. Palaeogeogr. Palaeoclimatol. Palaeoecol. 490, 571–578. https://doi.org/10.1016/j.palaeo.2017.11.045.
Faith, J.T., Potts, R., Plummer, T.W., Bishop, L.C., Marean, C.W., Tryon, C.A., 2012. New perspectives on middle Pleistocene change in the large mammal faunas of East Africa: Damaliscus hypsodon sp. nov. (Mammalia, Artiodactyla) from Lainyamok, Kenya. Palaeogeogr. Palaeoclimatol. Palaeoecol. 361–362, 84–93. https://doi.org/10.1016/j.palaeo.2012.08.005.
Farquhar, G.D., Ehleringer, J.R., Hubick, K.T., 1989. Discrimination and photosynthesis. Annu. Rev. Plant Physiol. Plant Mol. Biol. 40, 503–537.
Feng, Q.L., Zhu, X., Li, H.D., Kim, T.N., 2001. Crystal orientation regulation in ostrich eggshells. J. Cryst. Growth 233, 548–554. https://doi.org/10.1016/S0022-0248(01)01611-6.
Gliganic, L.A., Jacobs, Z., Roberts, R.G., Domínguez-Rodrigo, M., Mabulla, A.Z.P., 2012. New ages for Middle and Later Stone Age deposits at Mumba rockshelter, Tanzania: optically stimulated luminescence dating of quartz and feldspar grains. J. Hum. Evol. 62, 533–547. https://doi.org/10.1016/j.jhevol.2012.02.004.
Gramly, R.M., 1976. Upper Pleistocene Archaeological Occurrences at Site GvJm/22, Lukenya Hill, Kenya. In: New Series, vol 11. Royal Anthropological Institute of Great Britain and Ireland, pp. 319–344.
Hartman, A.T., 2018. An analysis of the effects of temperatures and circulations on the strength of the low-level jet in the Turkana Channel in East Africa. Theor. Appl. Climatol. 132, 1003–1017. https://doi.org/10.1007/s00704-017-2121-x.
Henshilwood, C.S., van Niekerk, K.L., Wurz, S., Delagnes, A., Armitage, S.J., Rifkin, R.F., Douze, K., Keene, P., Haaland, M.M., Reynard, J., Discamps, E., Mienies, S.S., 2014. Klipdrift Shelter, southern cape, South Africa: preliminary report on the howiesons poort layers. J. Archaeol. Sci. 45, 284–303. https://doi.org/10.1016/j.jas.2014.01.033.
Hobson, K.A., Clark, R.G., 1992. Assessing avian diets using stable isotopes I : turnover of ^{13}C in tissues. Condor 94, 181–188.
Högberg, P., 1997. Tansley Review No . ^{15}N natural abundance in soil – plant systems. New Phytol. 137, 179–203. https://doi.org/10.1046/j.1469-8137.1997.00808.x.
Hogg, A.G., Hua, Q., Blackwell, P.G., Niu, M., Buck, C.E., Guilderson, T.P., Heaton, T.J., Palmer, J.G., Reimer, P.J., Reimer, R.W., Turney, C.S.M., Zimmerman, S.R.H., 2013. SHCal13 southern hemisphere calibration, 0–50,000 Years cal BP. Radiocarbon 55, 1889–1903. https://doi.org/10.2458/azu_js_rc.55.16783.
Hut, G., 1987. Consultants' Group Meting on Stable Isotope Reference Samples for Geochemical and Hydrological Investigations (Vienna, Austria).
Inskeep, R.R., 1962. The age of the Kondoa rock paintings in light of recent excavations at Kisese II rock shelter. In: Mortelmans, G., Nenquin, J. (Eds.), Actes Du IVe Congres Panafrican de Prehistorie et de l'ectude Du Quaternaire. Tervuren, pp. 249–256.
Janz, L., Elston, R.G., Burr, G.S., 2009. Dating North Asian surface assemblages with ostrich eggshell: implications for palaeoecology and extirpation. J. Archaeol. Sci. 36, 1982–1989. https://doi.org/10.1016/j.jas.2009.05.012.
Johnson, B.J., Fogel, M.L., Miller, G.H., 1998. Stable isotopes in modern ostrich eggshell: a calibration for paleoenviromental applications in semi-arid regions of southern Africa. Geochem. Cosmochim. Acta 62, 2451–2461.
Johnson, B.J., Miller, G.H., Fogel, M.L., Beaumont, P.B., 1997. The determination of late Quaternary palaeoenvironments at Equus Cave, South Africa, using stable isotopes and amino acid racemization in ostrich eggshell. Palaeogeogr. Palaeoclimatol. Palaeoecol. 136, 121–137. https://doi.org/10.1016/S0031-0182(97)00043-6.
Johnson, T.C., 2017. Quaternary *Climate* Variation in Eastern Africa 1, 1–26. In:

Oxford Research Encyclopedia of Climate Science. https://doi.org/10.1093/acrefore/9780190228620.013.525.
Johnson, T.C., Werne, J.P., Brown, E.T., Abbott, A., Berke, M., Steinman, B.A., Halbur, J., Contreras, S., Grosshuesch, S., Deino, A., Lyons, R.P., Scholz, C.A., Schouten, S., Damsté, J.S.S., 2016. A progressively wetter climate in southern East Africa over the past 1.3 million years. Nature 537, 220–224. https://doi.org/10.1038/nature19065.
Jones, S.C., Stewart, Brian A. (Eds.), 2016. Africa from MIS 6-2. Springer. https://doi.org/10.1007/978-94-017-7520-5.
Kahmen, A., Sachse, D., Arndt, S.K., Tu, K.P., Farrington, H., Vitousek, P.M., Dawson, T.E., 2011. Cellulose $\delta^{18}O$ is an index of leaf-to-air vapor pressure difference (VPD) in tropical plants. Proc. Natl. Acad. Sci. 108, 1981–1986. https://doi.org/10.1073/pnas.1018906108.
Keeling, C.D., 1979. The Suess effect: 13Carbon-14Carbon interrelations. Environ. Int. 2, 229–300. https://doi.org/10.1016/0160-4120(79)90005-9.
Keeling, R.F., Graven, H.D., Welp, L.R., Resplandy, L., Bi, J., Piper, S.C., Sun, Y., Bollenbacher, A., Meijer, H.A.J., 2017. Atmospheric evidence for a global secular increase in carbon isotopic discrimination of land photosynthesis. Proc. Natl. Acad. Sci. 114, 10361–10366. https://doi.org/10.1073/pnas.1619240114.
Kelly, R.L., 2013. The Lifeways of Hunter-Gatherers: the Foraging Spectrum. Cambridge University Press, Cambridge.
Klein, R.G., 2008. Out of Africa and the evolution of human behavior. Evol. Anthropol. 17, 267–281. https://doi.org/10.1002/evan.20181.
Koch, P.L., 1998. Isotopic reconstruction of past continental environments. Annu. Rev. Earth Planet Sci. 26, 573–613. https://doi.org/10.1146/annurev.earth.26.1.573.
Kohn, M.J., 2010. Carbon isotope compositions of terrestrial C_3 plants as indicators of (paleo)ecology and (paleo)climate. Proc. Natl. Acad. Sci. 107, 19691–19695. https://doi.org/10.1073/pnas.1004933107.
Kohn, M.J., 1996. Predicting animal $\delta^{18}O$: accounting for diet and physiological adaptation. Geochem. Cosmochim. Acta 60, 4811–4829.
Lee-Thorp, J.A., Ecker, M., 2015. Holocene environmental change at wonderwerk Cave, South Africa: insights from stable light isotopes in ostrich eggshell. Afr. Archaeol. Rev. 32, 793–811. https://doi.org/10.1007/s10437-015-9202-y.
Leuthold, W., 1976. Notes on the breeding Biology of the ostrich Struthio Camelus in tsavo east national park, Kenya. Ibis (Lond. 1859) 541–544.
Levin, N.E., Cerling, T.E., Passey, B.H., Harris, J.M., Ehleringer, J.R., 2006. A stable isotope aridity index for terrestrial environments. Proc. Natl. Acad. Sci. 103, 11201–11205. https://doi.org/10.1073/pnas.0604719103.
Lind, E.M., Morrison, M.E.S., 1974. East African Vegetation (London).
Luz, B., Barkan, E., 2011. The isotopic composition of atmospheric oxygen. Glob. Biogeochem. Cycles 25, 1–14. https://doi.org/10.1029/2010GB003883.
Luz, B., Kolodny, Y., Horowitz, M., 1984. Fractionation of oxygen isotopes between mammalian bone-phosphate and environmental drinking water. Geochem. Cosmochim. Acta 48, 1689–1693.
Marean, C.W., 1992. Implications of Late Quaternary mammalian fauna from Lukenya Hill (South-Central Kenya) for paleoenvironmental change and Faunal extinctions Kenya. Quat. Res. 255, 239–255.
Mallick, S., Li, H., Lipson, M., Mathieson, I., Gymrek, M., Racimo, F., Zhao, M., Chennagiri, N., Nordenfelt, S., Tandon, A., Skoglund, P., Lazaridis, I., Sankararaman, S., Fu, Q., Rohland, N., Renaud, G., Erlich, Y., Willems, T., Gallo, C., Spence, J.P., Song, Y.S., Poletti, G., Balloux, F., van Driem, G., de Knijff, P., Romero, I.G., Jha, A.R., Behar, D.M., Bravi, C.M., Capelli, C., Hervig, T., Moreno-Estrada, A., Posukh, O.L., Balanovska, E., Balanovsky, O., Karachanak-Yankova, S., Sahakyan, H., Toncheva, D., Yepiskoposyan, L., Tyler-Smith, C., Xue, Y., Abdullah, M.S., Ruiz-Linares, A., Beall, C.M., Di Rienzo, A., Jeong, C., Starikovskaya, E.B., Metspalu, E., Parik, J., Villems, R., Henn, B.M., Hodoglugil, U., Mahley, R., Sajantila, A., Stamatoyannopoulos, G., Wee, J.T.S., Khusainova, R., Khusnutdinova, E., Litvinov, S., Ayodo, G., Comas, D., Hammer, M.F., Kivisild, T., Klitz, W., Winkler, C.A., Labuda, D., Bamshad, M., Jorde, L.B., Tishkoff, S.A., Watkins, W.S., Metspalu, M., Dryomov, S., Sukernik, R., Singh, L., Thangaraj, K., Pääbo, S., Kelso, J., Patterson, N., Reich, D., 2016. The Simons Genome Diversity Project: 300 genomes from 142 diverse populations. Nature 538, 201–206. https://doi.org/10.1038/nature18964.
Marean, C.W., 1991. Late Quaternary Paleoenvironments and Faunal Exploitation in East Africa. University of California Berkeley.
Marean, C.W., Gifford-Gonzalez, D., 1991. Late Quaternary extinct ungulates of East Africa and paleoenvironmental implications. Nature 350, 418–420.
McGee, D., deMenocal, P.B., 2017. Climatic Changes and Cultural Responses during the African Humid Period Recorded in Multi-Proxy Data. In: Oxford Research Encyclopedia of Climate Science. https://doi.org/10.1093/acrefore/9780190228620.013.529.
McGee, D., deMenocal, P.B., Winckler, G., Stuut, J.B.W., Bradtmiller, L.I., 2013. The magnitude, timing and abruptness of changes in North African dust deposition over the last 20,000 yr. Earth Planet. Sci. Lett. 371–372, 163–176. https://doi.org/10.1016/j.epsl.2013.03.054.
McSweeney, C., New, M., Lizcano, G., 2010. The UNDP climate change country profiles improving the accessibility of observed and projected climate information for studies of climate change in developing countries. Bull. Am. Meteorol. Soc. 91, 157–166.
McSweeney, C., New, M., Lizcano, G., 2012a. UNDP Climate Change Country Profiles: Tanzania, UNDP Climate Change Country ProfilesCountry Profiles. UNDP. http://country-profiles.geog.ox.ac.uk/.
McSweeney, C., New, M., Lizcano, G., 2012a. UNDP Climate Change Country Profiles: Kenya, UNDP Climate Change Country Profiles. UNDP. http://country-profiles.geog.ox.ac.uk/.
Mikhailov, K.E., 1997. Fossil and recent eggshell in amniotic vertebrates: fine structure, comparative morphology and classification. Spec. Pap. Palaeontol. 56, 1–80.
Miller, G., Magee, J., Smith, M., Spooner, N., Baynes, A., Lehman, S., Fogel, M., Johnston, H., Williams, D., Clark, P., Florian, C., Holst, R., DeVogel, S., 2016. Human predation contributed to the extinction of the Australian megafaunal bird Genyornis newtoni ~47 ka. Nat. Commun. 7, 1–7. https://doi.org/10.1038/ncomms10496.
Miller, G.H., Fogel, M.L., 2016. Calibrating δ18O in Dromaius novaehollandiae (emu) eggshell calcite as a paleo-aridity proxy for the Quaternary of Australia. Geochem. Cosmochim. Acta 193, 1–13. https://doi.org/10.1016/j.gca.2016.08.004.
Milton, S.J., Dean, R.J., Siegfried, W.R., 1994. Food selection by ostrich in southern africa. J. Wildl. Manag. 58, 234–248.
Moran, V., Hoffmann, J., Donnelly, D., van Wilgen, B., Zimmermann, H., 2000. Biological control of alien, invasive pine trees (Pinus species) in South Africa. Proc. X Int. Symp. Biol. Control Weeds. Mont. State Univ. Bozeman, Mont. USA 953, 941–953.
Moreau, R.E., 1950. The breeding seasons of african birds. Int. J. Avian Sci. 223–267.
Newsome, S.D., Miller, G.H., Magee, J.W., Fogel, M.L., 2011. Quaternary record of aridity and mean annual precipitation based on δ15N in ratite and dromornithid eggshells from Lake Eyre, Australia. Oecologia 167, 1151–1162. https://doi.org/10.1007/s00442-011-2046-5.
Nicholson, S., 2016. The Turkana low-level jet: mean climatology and association with regional aridity. Int. J. Climatol. 36, 2598–2614. https://doi.org/10.1002/joc.4515.
Nicholson, S.E., 2017. Climate and climatic variability of rainfall over eastern Africa. Rev. Geophys. 55, 590–635. https://doi.org/10.1002/2016RG000544.
Niespolo, E.M., Sharp, W.D., Fylstra, N.D., Avery, G., Blegen, N., Faith, J.T., Henshilwood, C.S., Klein, R., Van Niekerk, K., Weisz, D.G., Tryon, C.A., 2018. U-Th Burial Dating of Ostrich Eggshell beyond the 14C Limit. Geochemical Society, Boston, MA.
Niespolo, E.M., Sharp, W.D., Tryon, C.A., Faith, J.T., Miller, M.J., Dawson, T.E., 2015. C and N Isotopes in Ostrich Eggshell as Proxies of Paleovegetation and Paleoprecipitation: Extraction, Preservation, and Application to Pleistocene Archaeological Samples. American Geophysical Union, San Francisco, CA.
Nys, Y., Gautron, J., Garcia-Ruiz, J.M., Hincke, M.T., 2004. Avian eggshell mineralization: biochemical and functional characterization of matrix proteins. Comptes Rendus Palevol 3, 549–562. https://doi.org/10.1016/j.crpv.2004.08.002.
Nys, Y., Hincke, M.T., Arias, J.L., Garcia-Ruiz, J.M., Solomon, S.E., 1999. Avian eggshell mineralization. Avian Poultry Biol. Rev. 10, 143–166.
Owen, B.R., Renaut, R.W., Muiruri, V.M., Rabideaux, N.M., Lowenstein, T.K., McNulty, E.P., Leet, K., Deocampo, D., Luo, S., Deino, A.L., Cohen, A., Sier, M.J., Campisano, C., Shen, C.-C., Billingsley, A., Mbuthia, A., Stockhecke, M., 2019. Quaternary history of the Lake Magadi basin, southern Kenya rift: tectonic and climatic controls. Palaeogeogr. Palaeoclimatol. Palaeoecol. 518, 97–118. https://doi.org/10.1016/j.palaeo.2019.01.017.
Owen, R.B., Muiruri, V.M., Lowenstein, T.K., Renaut, R.W., Rabideaux, N., Luo, S., Deino, A.L., Sier, M.J., Dupont-Nivet, G., McNulty, E.P., Leet, K., Cohen, A., Campisano, C., Deocampo, D., Shen, C.-C., Billingsley, A., Mbuthia, A., 2018. Progressive aridification in East Africa over the last half million years and implications for human evolution. Proc. Natl. Acad. Sci. 115, 11174–11179. https://doi.org/10.1073/pnas.1801357115.
Passey, B.H., Hu, H., Ji, H., Montanari, S., Li, S., Henkes, G.A., Levin, N.E., 2014. Triple oxygen isotopes in biogenic and sedimentary carbonates. Geochem. Cosmochim. Acta 141, 1–25. https://doi.org/10.1016/j.gca.2014.06.006.
Petit, J.R., Jouzel, J., Raynaud, D., Barkov, N.I., Barnola, J.-M., Bassile, I., Bender, M., Chappellaz, J., Davis, M., Delaygue, G., Delmotte, M., Kotlyakov, V.M., Legrand, M., Lipenkov, V.Y., Lorius, C., Ritz, L.P.C., Saltzman, E., Stievenard, M., 1999. Climate and atmospheric history of the past 420,000 years from the Vostock ice core, Antarctica. Nature 399, 429–439.
R Core Team, 2018. R: A Language and Environment for Statistical Computing.
Reimer, P.J., Bard, E., Bayliss, A., Beck, J.W., Blackwell, P.G., Ramsey, C.B., Buck, C.E., Cheng, H., Edwards, R.L., Friedrich, M., Grootes, P.M., Guilderson, T.P., Haflidason, H., Hajdas, I., Hatté, C., Heaton, T.J., Hoffmann, D.L., Hogg, A.G., Hughen, K.A., Kaiser, K.F., Kromer, B., Manning, S.W., Niu, M., Reimer, R.W., Richards, D.A., Scott, E.M., Southon, J.R., Staff, R.A., Turney, C.S.M., van der Plicht, J., 2013. IntCal13 and Marine13 radiocarbon age calibration curves 0–50,000 Years cal BP. Radiocarbon 55, 1869–1887. https://doi.org/10.2458/azu_js_rc.55.16947.
Roberts, P., Henshilwood, C.S., Van Niekerk, K.L., Keene, P., Gledhill, A., Reynard, J., Badenhorst, S., Lee-Thorp, J., 2016. Climate, environment and early human innovation: stable isotope and faunal proxy evidence from archaeological sites (98-59ka) in the southern Cape, South Africa. PLoS One 11, 1–20. https://doi.org/10.1371/journal.pone.0157408.
Robinson, J.R., 2017. Thinking locally: environmental reconstruction of Middle and Later Stone Age archaeological sites in Ethiopia, Kenya, and Zambia based on ungulate stable isotopes. J. Hum. Evol. 106, 19–37. https://doi.org/10.1016/j.jhevol.2017.01.013.
Roden, J.S., Ehleringer, J.R., 1999. Observations of hydrogen and oxygen isotopes in leaf water confirm the craig-gordon model under wide-ranging environmental conditions. Plant Physiol. 120, 1165–1174. https://doi.org/10.1104/pp.120.4.1165.
Santos, G.M., Southon, J.R., Druffel-Rodriguez, K.C., Griffin, S., Mazon, M., 2004. Magnesium Perchlorate as an alternative water trap in AMS graphite sample preparation: a report on sample preparation at KCCAMS at the University of

California, Irvine. Radiocarbon 46, 165–173.
Schefuß, E., Schouten, S., Schneider, R.R., 2005. Climatic controls on central African hydrology during the past 20,000 years. Nature 437, 1003–1006. https://doi.org/10.1038/nature03945.
Schmidt-Nielsen, K., Kanwisher, J., Lasiewski, R.C., Cohn, J.E., Bretz, W.L., 1969. Temperature regulation and respiration in the ostrich. Condor 71, 341–352.
Ségalen, L., Lee-Thorp, J.A., 2009. Palaeoecology of late Early Miocene fauna in the Namib based on 13C/12C and 18O/16O ratios of tooth enamel and ratite eggshell carbonate. Palaeogeogr. Palaeoclimatol. Palaeoecol. 277, 191–198. https://doi.org/10.1016/j.palaeo.2009.03.018.
Segalen, L., Renard, M., Pickford, M., Senut, B., Cojan, I., Le Callonnec, L., Rognon, P., 2002. Environmental and climatic evolution of the Namib Desert since the Middle Miocene: the contribution of carbon isotope ratios in ratite eggshells. Compt. Rendus Geosci. 334, 917–924. https://doi.org/10.1016/S1631-0713(02)01837-0.
Shanahan, T.M., Mckay, N.P., Hughen, K.A., Overpeck, J.T., Otto-Bliesner, B., Heil, C.W., King, J., Scholz, C.A., Peck, J., 2015. The time-transgressive termination of the African humid period. Nat. Geosci. 8, 140–144. https://doi.org/10.1038/ngeo2329.
Sharp, W., Fylstra, N.D., Tryon, C.A., Faith, J.T., Peppe, D.J., 2016. U-Th burial dating of ostrich eggshell: a new geochronometer for African archaeological sites. Quat. Int. 404, 198–199. https://doi.org/10.1016/j.quaint.2015.08.171.
Sharp, W.D., Tryon, C.A., Niespolo, E.M., Fylstra, N.D., Tripathy-Lang, A., Faith, J.T., 2019. 230Th/U burial dating of ostrich eggshell. Quat. Sci. Rev. 219, 362–276.
Shorrocks, B., 2007. The Biology of African Savannahs (Oxford).
Sinclair, A.R.E., 1978. Factors affecting the food supply and breeding season of resident birds and movements of palaearctic migrants in a tropical african savannah. Ibis (Lond. 1859) 480–497. https://doi.org/10.1016/j.brainres.2015.10.018.
Stern, L.A., Johnson, G.D., Chamberlain, C.P., 1994. Carbon isotope signature of environmental change found in fossil ratite eggshells from a South Asian Neogene sequence. Geology 22, 419–422.
Sternberg, L.O., Deniro, M.J., Johnson, H.B., 1984. Isotope ratios of cellulose from plants having different photosynthetic pathways. Plant Physiol. 74, 557–561. https://doi.org/10.1104/pp.74.3.557.
Sternberg, L.S.L., 1989. Oxygen and hydrogren isotope ratios in plant cellulose: mechanisms and applications. In: Rundel, P.W. (Ed.), Stable Isotopes in Ecological Research. University of California Press, pp. 124–141.
Texier, P.J., Porraz, G., Parkington, J., Rigaud, J.P., Poggenpoel, C., Tribolo, C., 2013. The context, form and significance of the MSA engraved ostrich eggshell collection from Diepkloof Rock Shelter, Western Cape, South Africa. J. Archaeol. Sci. 40, 3412–3431. https://doi.org/10.1016/j.jas.2013.02.021.
Tierney, J.E., deMenocal, P.B., Zander, P.D., 2017. A climatic context for the out-of-Africa migration. Geology 45, 1023–1026. https://doi.org/10.1130/G39457.1.
Tierney, J.E., Lewis, S.C., Cook, B.I., LeGrande, A.N., Schmidt, G.A., 2011a. Model, proxy and isotopic perspectives on the east african Humid Period. Earth Planet. Sci. Lett. 307, 103–112. https://doi.org/10.1016/j.epsl.2011.04.038.
Tierney, J.E., Russell, J.M., Sinninghe Damsté, J.S., Huang, Y., Verschuren, D., 2011b. Late quaternary behavior of the east african monsoon and the importance of the Congo air boundary. Quat. Sci. Rev. 30, 798–807. https://doi.org/10.1016/j.quascirev.2011.01.017.
Timmermann, A., Friedrich, T., 2016. Late Pleistocene climate drivers of early human migration. Nature 538, 92–95. https://doi.org/10.1038/nature19365.
Tryon, C.A., 2019. the east african middle/later stone age transition and cultural dynamics of the late pleistocene. Evol. Anthropol. 28, 267–282.
Tryon, C.A., Crevecoeur, I., Faith, J.T., Ekshtain, R., Nivens, J., Patterson, D., Mbua, E.N., Spoor, F., 2015. Late Pleistocene age and archaeological context for the hominin calvaria from GvJm-22 (Lukenya Hill, Kenya). Proc. Natl. Acad. Sci. 112, 2682–2687. https://doi.org/10.1073/pnas.1417909112.
Tryon, C.A., Faith, J.T., 2016. A demographic perspective on the middle to later stone age transition from nasera rockshelter, Tanzania. Philos. Trans. R. Soc. Biol. Sci. 371 https://doi.org/10.1098/rstb.2015.0238.
Tryon, C.A., Faith, J.T., 2013. Variability in the middle stone age of eastern africa. Curr. Anthropol. 54, S234–S254. https://doi.org/10.1023/A:1008961314500.
Tryon, C.A., Lewis, J.E., Ranhorn, K., 2019. Excavating the archives: the 1956 excavation of the late pleistocene-holocene sequence at kisese II (Tanzania). In: Sahle, Y., Reyes-Centeno, H., Bentz, C. (Eds.), Modern Human Origins and Dispersal. Kerns Verlag, Tubingen, pp. 215–238.
Tryon, C.A., Lewis, J.E., Ranhorn, K.L., Kwekason, A., Alex, B., Laird, M.F., Marean, C.W., Niespolo, E., Nivens, J., Mabulla, A.Z.P., 2018. Middle and later stone age chronology of kisese II rockshelter (UNESCO World Heritage Kondoa Rock-Art Sites), Tanzania. PLoS One 13. https://doi.org/10.1371/journal.pone.0192029.
van Breugel, P., Kindt, R., Lillesø, J., Bingham, M., Demissew, S., Dudely, C., Friis, I., Gachathi, F., Kalema, J., Mbago, F., Moshi, H., Muluma, J., Namaganda, M., Ndangalasi, H., Ruffo, C., Vedaste, M., Jamnadass, R., 2015. Potential Natural Vegetation Map of Eastern Africa (Burundi, Ethiopia, Kenya, Malawi, Rwanda, Tanzania, Uganda and Zambia). Version 2.0. [WWW Document]. For. Landsc. World Agrofor. Cent. (ICRAF).
Verschuren, D., Sinninghe Damsté, J.S., Moernaut, J., Kristen, I., Blaauw, M., Fagot, M., Haug, G.H., 2009. Half-precessional dynamics of monsoon rainfall near the East African Equator. Nature 462, 637–641. https://doi.org/10.1038/nature08520.
Vogel, J.C., 1983. Isotopic evidence for the past climates and vegetation of southern Africa. Bothalia 14, 391–394. https://doi.org/10.4102/abc.v14i3/4.1183.
Von Schirnding, Y., Van der Merwe, N.J., Vogel, J.C., 1982. Influence of diet and age on carbon isotope ratios in ostrich. eggshell 24, 3–20.
West, J.B., Sobek, A., Ehleringer, J.R., 2008. A simplified GIS approach to modeling global leaf water isoscapes. PLoS One 3. https://doi.org/10.1371/journal.pone.0002447.
White, F., 1983. The Vegetation of Africa. A Descriptive Memoir to Accompany the UNESCO/AETFAT/UNSO Vegetation Map of Africa. UNESCO, Paris.
Williams, J.B., Siegfried, W.R., Milton, S.J., Adams, N.J., Dean, W.R.J., du Plessis, M.A., Jackson, S., 1993. Field metabolism , water requirements , and foraging behavior of wild ostriches in the namib. Ecology 74, 390–404.
Wilmsen, E.N., 2015. Ostrich eggshells and their beads. South african archaeol. Bull. (Arch. Am. Art) 70, 89–105.
Ziegler, M., Simon, M.H., Hall, I.R., Barker, S., Stringer, C., Zahn, R., 2013. Development of Middle Stone Age innovation linked to rapid climate change. Nat. Commun. 4, 1905–1909. https://doi.org/10.1038/ncomms2897.